# Breast tumor Insulin-like growth factor receptor regulates cell adhesion and metastasis: Alignment of mouse single cell and human breast cancer transcriptomics

Alison E. Obr[1], Yung-Jun Chang[2], Virginia Ciliento[1], Alexander Lemenze[3], Krystopher Maingrette[1], Joseph J. Bulatowicz[1], Quan Shang[1], Emily Gallagher[4], Derek LeRoith[4] and Teresa L. Wood[1*]

[1]Department of Pharmacology, Physiology & Neuroscience, New Jersey Medical School, Rutgers University, Newark, New Jersey

[2]Office of Advance Research Computing, Rutgers University, Piscataway, New Jersey

[3]Department of Pathology, New Jersey Medical School, Rutgers University, Newark, New Jersey

[4]Division of Endocrinology, Diabetes and Bone Diseases, The Samuel Bronfman Department of Medicine, Icahn Sinai School of Medicine at Mt. Sinai, New York, New York 10029

**Running Title:** IGF-1R Promotes Cell Adhesion and Reduces Tumor Metastasis

**Key Words:** IGF-1R, breast cancer, cell adhesion, metastasis, cadherin, METABRIC

**Financial Support:** This work was supported by Public Health Service National Institutes of Health grants NCI R01CA204312 (T.L.W) and NCI R01CA128799 (D.L.), New Jersey Commission on Cancer Research Postdoctoral Fellowship DFHS15PPC039 and American Cancer Society-Fairfield County Roast Postdoctoral Fellowship 130455-PF-17-244-01-CSM (A.E.O.).

***Corresponding Author**

Teresa L. Wood

Dept. Pharmacology, Physiology & Neuroscience

New Jersey Medical School, Rutgers University

Cancer Institute of New Jersey - Newark

205 S. Orange Ave / H1200

Newark, NJ 07103

Phone: 973-972-6529

Email: terri.wood@rutgers.edu

The authors declare no potential conflicts of interest.

Word count: 5790

Number of Figures: 8

**Abstract**

The acquisition of a metastatic phenotype is the critical event that determines patient survival from breast cancer. Several receptor tyrosine kinases have functions both in promoting and inhibiting metastasis in breast tumors. Although the insulin-like growth factor 1 receptor (IGF-1R) has been considered a target for inhibition in breast cancer, low levels of IGF-1R expression are associated with worse overall patient survival. To determine how reduced IGF-1R impacts tumor phenotype, we used weighted gene correlation network analysis (WGCNA) of METABRIC patient data and identified gene modules specific to cell cycle, adhesion, and immune cell signaling inversely correlated with IGF-1R expression in human breast cancers. Integration of human patient data with data from mouse tumors revealed similar pathways necessary for promoting metastasis in basal-like tumors with reduced signaling or expression of the IGF-1R. Functional analyses revealed the basis for the enhanced metastatic phenotype including alterations in E- and P-cadherins.

17 **Main**

18 Metastasis is the leading cause of cancer patient death. Several individual genes
19 and associated cellular pathways contribute to a metastatic phenotype but the
20 mechanisms that cause some tumors to become metastatic are still poorly understood.
21 Receptor tyrosine kinases (RTKs) have been implicated in promoting metastatic
22 properties in tumor cells. RTK domain mutations are not a prominent feature in most
23 cancers; instead, RTK expression level is the general driver of tumorigenesis and
24 metastasis (1-4). A well-known RTK that has a prominent role in a subclass of breast
25 cancers and has been the focus for successful cancer therapeutics is HER2. However,
26 targeting several other RTKs including the epidermal growth factor receptor (EGFR) and
27 the insulin-like growth factor receptor (IGF-1R) in breast tumors has been mostly
28 unsuccessful (2, 5, 6). The emerging theme for these receptors is their context-
29 dependent functions that change whether they are growth-promoting or growth-
30 inhibiting in the primary tumor or metastatic environment.

31 Expression of IGF-1R has been implicated in tumor oncogenesis by promoting
32 tumor cell proliferation and survival (7-9). Due to this oncogenic function, several IGF-
33 1R inhibitors have been developed and used in clinical trials. While IGF-1R was a clear
34 target, the inhibitors were largely unsuccessful in the clinic (5, 6). There is now clear
35 evidence that the IGF-1R also has tumor or metastasis suppressive functions; IGF-1R
36 expression in breast tumors correlates with positive overall patient survival and a more
37 differentiated tumor phenotype (10-12). Consistent with these data, recent reports using
38 the TCGA and METABRIC patient databases have revealed low IGF-1R expression is

39 associated with undifferentiated, triple-negative breast cancer (TNBC) and worse overall
40 survival (13, 14).
41 In the present study, we utilized the METABRIC patient database and single-cell
42 RNA sequencing of two IGF-1R loss-of-function mouse tumor models to uncover how
43 IGF-1R signaling regulates intrinsic epithelial cell signaling to suppress metastasis. We
44 identify key pathways necessary for promoting metastasis including upregulation of
45 immune cell activation signals, cell cycle dysregulation, and altered cell adherence and
46 show that IGF-1R is required to maintain a metastasis suppressive tumor
47 microenvironment. We further show that adherence between luminal and basal tumor
48 cells is necessary for tumor growth at the secondary site and that reduced IGF-1R
49 signaling in tumor epithelial cells dysregulates E- and P-cadherin resulting in reduced
50 cell adhesion.
51
52 **Methods**
53 **Animal Models**
54 All animal protocols were approved by the Rutgers University Institutional Animal
55 Care and Use Committee (Newark, NJ) and all experiments were managed in
56 accordance with the NIH guidelines for the care and use of laboratory animals. Animal
57 care was provided by the veterinary staff of the division of animal resources in the New
58 Jersey Medical School Cancer Center of Rutgers Biomedical Health Sciences. The
59 *MMTV-Wnt1* line on an FVB background [FVB.Cg-Tg(Wnt1)1Hev/J] was obtained as a

60 gift from Dr. Yi Li. The *MMTV-Wnt1//MMTV-dnIgf1r* (referred to here as DN-Wnt1) line
61 was described previously (15).
62 Mice carrying floxed alleles of exon 3 of the *Igf1r* gene (16) were bred with a
63 keratin 8 (K8)-Cre$^{ERT}$ transgenic line (JAX stock #017947) (17) and with the *MMTV-*
64 *Wnt1* transgenic line to produce female mice that were homozygous for the *Igf1r* floxed
65 alleles and hemizygous for both the K8-Cre$^{ERT}$ and *MMTV-Wnt1* transgenes referred to
66 as K8iKOR-Wnt1 mice (see Supplemental Methods).
67
68 **Mammary Tumor Epithelial Cell Dissociation**
69 Tumor mammary epithelial cells (MECs) were isolated from Wnt1, DN-Wnt1, and
70 K8iKOR-Wnt1 mice similarly to our prior study (15). Whole tumors were excised and
71 dissociated with the gentleMACs tissue dissociator (130-093-235, protocol m_TDK2)
72 and mouse specific tumor dissociation kit (Miltenyi, 130-096-730). Organoids that retain
73 basement membrane attachments were trypsinized (0.05% Trypsin-EDTA, Gibco) and
74 filtered with a 40 μm cell strainer (BD Biosciences) to isolate a single cell suspension of
75 dissociated tumor MECs (see also Supp. Methods). Isolated tumor MECs were counted
76 with a hemocytometer for flow cytometry, FACS, tail vein injections (TVIs), *in vitro*
77 adhesion assays, and cell culture assays.
78
79 **Tail vein injection (TVI) of primary tumor epithelial cells**
80 Tumor MECs were isolated as described above (n=4) and injected at $1x10^6$
81 cells/200ul PBS (unsorted) or $0.25x10^6$ cells/200ul (sorted) into the tail vein of 6-week-

82 old eGFP mice (n=4). Animals were perfused with 3% PFA and lungs were harvested at
83 1-, 3-, 6-, 8-, and 12-weeks post injections. After perfusion, harvested lungs were drop-
84 fixed in 4% PFA overnight and dehydrated with 70% EtOH for paraffin embedding. For
85 TVIs with flow sorted tumor MECs (n=3), $0.25x10^6$ luminal ($CD24^+/CD29^{lo}$), basal
86 ($CD24^+/CD29^{hi}$), or unsorted epithelial cells/200ul PBS were injected into eGFP mice
87 (n=3); lungs were harvested and processed 1-week post injection (wpi).
88
89 **RNA isolation and real-time quantitative PCR**
90 RNA was purified from whole tumor and sorted tumor epithelial cells according to
91 the manufacturer's protocol (Qiagen). RNA concentration and quality was assayed with
92 the NanoDrop ND-1000 (Thermo Scientific). Sorted tumor epithelial cell cDNA was
93 transcribed according to manufacturer's protocol using SuperScript II (Invitrogen) from
94 total RNA (200 ng). Samples were run in technical triplicate to determine relative gene
95 expression by real-time quantitative PCR (qRT-PCR) detected with SsoAdvanced
96 Universal SYBR Green Supermix (BioRad) using the BioRad CFX96 real-time PCR
97 machine according to manufacturer's instructions. Transcript levels were normalized to
98 glyceraldehyde-3-phosphate dehydrogenase (GAPDH) or Gusb for mouse and ß-actin
99 for human, and data were analyzed using the Q-Gene software (BioTechniques
100 Software Library) (18). For detection of the *Igf1r*-deleted allele in isolated cell
101 populations, we amplified the corresponding fragment from the coding region of the
102 messenger RNA specific for the inactivated receptor allele. The forward primer
103 annealed with exon 2 and the reverse primer spanned the knockout-specific splice

104 junction between exons 2 and 4. Primer oligonucleotide pairs for qRT-PCR are provided
105 (Supp. Table 1).
106
107 **Histology and Immunofluorescence**
108 Tumor tissues and lungs from animals with primary tumors (n=4 per genotype)
109 were drop-fixed in 4% paraformaldehyde (PFA), embedded in paraffin, and sectioned at
110 7 $\mu$m. Lung sections from animals with primary tumors or from TVIs were used for
111 hematoxylin and eosin staining. Tumor and lung sections were processed for antigen
112 retrieval for immunofluorescence (IF) as described previously (19). Tissue sections
113 were immunostained with primary antibodies: E-cadherin (1:100; Invitrogen, ECCD-2),
114 cytokeratin-8 (1:100; TROMA-I, DSHB), cytokeratin-14 (1:250; Invitrogen, PA5-16722),
115 phospho-Histone H3 (Ser10) (1:200; Cell Signaling, D2C8 XP), P-cadherin (1:100;
116 Invitrogen, MA1-2003), and Ki67 (1:100; Vector Labs, VP-K451) and with species-
117 specific fluorochrome-conjugated secondary antibodies (1:500, Invitrogen).
118 A Keyence BZ-X all-in-one fluorescence microscope with BZ- scientific imaging
119 processing software (Keyence) was used to capture images. At least 5 individual fields
120 were captured at 20X or 40X magnification from tumor sections (n=4 per genotype). For
121 thicker sections, a z-stack range was acquired and the focus analysis was utilized to
122 obtain the deconvoluted image.
123
124 **Tumor epithelial cell *in vitro* adhesion assays**

125 Primary tumors were dissociated as described above and incubated in tissue
126 culture on collagen coated plates for 10 hours. Culture media (DMEM/F12, 5% FBS,
127 insulin (5 μg/mL), EGF (5 ng/mL), hydrocortisone (1 μg/mL), 0.1% gentimicin) was
128 removed and cells in suspension were fixed on slides using a cytospin (Shandon
129 Cytospin 3) for 10 minutes at 1500 rpm for immunofluorescence (IF). Cells attached to
130 the collagen matrix were fixed with 4% PFA for 10 minutes at room temperature for IF
131 analysis or lysed with RLT buffer (Qiagen) for RNA isolation and qRT-PCR analysis as
132 described above.
133 For IF, cells were processed for staining as previously described (20). Cells were
134 stained with primary antibodies: cytokeratin-8 (1:100; TROMA-I, DSHB) and cytokeratin-
135 14 (1:250; Invitrogen, PA5-16722) and with species-specific fluorochrome-conjugated
136 secondary antibodies (1:500, Invitrogen). To visualize cell nuclei, cells were stained with
137 DAPI (1:10,000 in PBS). Images were captured as described above and cells were
138 manually counted using ImageJ.
139
140 **Single-cell RNA sequencing**
141 Whole Wnt1 (tamoxifen injected, Cre negative), DN-Wnt1, and K8iKOR-Wnt1
142 tumors were dissociated as described above except tumor cells were filtered with a 70
143 μm filter directly after dissociation to collect single cells from the entire tumor. Cells were
144 captured using the 10X Chromium system (10X Genomics) and sequenced with the
145 NextSeq 500 (Illumina). Analysis is described in Supp. Methods.
146

147 **WGCNA analysis of METABRIC data for gene module identification**

148 The data generated from 1981 patients within the METABRIC project (21) was
149 used in this investigation. These data were accessed through Synapse
150 (synapse.sagebase.org), including normalized expression data and clinical feature
151 measurements. The associated expression Z scores were downloaded from cBioPortal
152 (https://www.cbioportal.org/). The method of weighted gene co-expression network
153 analysis (WGCNA) was used to identify gene modules with significant statistical
154 association to the phenotypic trait including patient age, tumor size, tumor grade, cancer
155 subtype, and IGF-1R expression. The description of clinical feature coding and gene
156 correlation analysis is found in Supp. Methods.

157

158 **Ingenuity Pathway Analysis (IPA)**

159 scRNA-seq: Differentially expressed gene sets were identified from the DN-Wnt1
160 and K8iKOR-Wnt1 compared to Wnt1 mouse tumors for each whole tumor and
161 epithelial cell specific cluster determined from scRNA-seq as described above. These
162 differentially expressed genes were used for IPA pathway enrichment and graphical
163 summary analysis. The top 5 pathways based on significance were plotted by percent
164 genes altered in each pathway. Graphical summaries were generated using the top
165 pathways, cell functions, and target genes identified from differentially expressed genes
166 (DN-Wnt1 vs. Wnt1; K8iKOR-Wnt1 vs. Wnt1) in each cluster.

167 WGCNA METABRIC analysis: Gene names and expression levels identified from
168 highly correlative co-expression gene modules as described in Supp. Methods were
169 uploaded into the IPA software (Qiagen) and analyzed for pathway enrichment. The top

170 5 pathways based on log-fold change significance for each module were plotted by
171 percent of total genes up- and down-regulated in each pathway.
172 Comparison Analysis: Whole tumor gene changes were compared to ME genes
173 where the output is pathway alterations. Here, exact genes were not completely similar,
174 but pathways were comparable.
175
176 **Statistics**
177 All graphical data were expressed as the mean ± SEM. Statistical comparisons
178 were carried out by GraphPad Prism9 software. The Student's *t*-test or non-parametric
179 Mann-Whitney U test was used for two-group comparisons. Specific comparisons are
180 described in figure legends when necessary. For multiple variable analysis, the One-Way
181 ANOVA with Tukey's Multiple Comparison post-hoc test was performed. For the tumor
182 growth curve and *in vitro* adhesion analysis, the non-linear regression least squares
183 regression for slope best fit was used to compare differences between each line. The Chi-
184 Square test was used to determine differences between genotypes in the metastasis
185 table. Power calculations were performed based on pilot data to determine the number of
186 tumor samples necessary using a 2-sided hypothesis test, an $\alpha = 0.0025$, and 80% power.
187
188 **Results**
189 *Low levels of IGF-1R correlate with a metastatic gene signature in breast cancer*
190 Recent analysis of TCGA and METABRIC databases have revealed IGF-1R
191 expression is reduced in TNBC (13, 14). Furthermore, low levels of IGF-1R predict

192 worse overall patient survival across all breast cancer subtypes (14, 22). Our previous
193 studies reported IGF-1R expression levels in human tumors are inversely correlated
194 with several key target genes that alter the tumor microenvironment (14) . These prior
195 expression analyses of human breast tumors with low IGF-1R were performed on genes
196 we identified as dysregulated with reduced IGF-1R signaling and associated with
197 increased metastasis in our mouse tumor model (14, 23). The findings from human and
198 mouse support the hypothesis that low expression of IGF-1R could be used to identify
199 gene signatures associated with aggressive breast cancers. To independently stratify
200 genes correlated with either low or high IGF-1R expression in human breast cancers,
201 we performed a global unbiased weighted gene co-expression network analysis
202 (WGCNA) utilizing the METABRIC database to identify gene expression modules
203 associated with IGF-1R expression Z-score, referred to as IGF1R gene set 1 (IGF1R-
204 GS1; Supp. Fig. 2).
205 Due to the large number of genes in the IGF1R-GS1, we refined our WGCNA
206 analyses to limit the original data set to those genes with the strongest positive or
207 negative correlation to IGF-1R expression (Fig. 1a). In this refined gene set (IGF1R-
208 GS2), we identified four gene co-expression modules significantly correlated with low
209 IGF-1R (correlation score ≤ -0.25), all of which were also associated with high tumor
210 grade and three of which were associated with TNBC. One module significantly
211 associated with high IGF-1R (correlation 0.61) was also associated with ER+/PR+
212 breast cancers and low tumor grade (Fig. 1a).

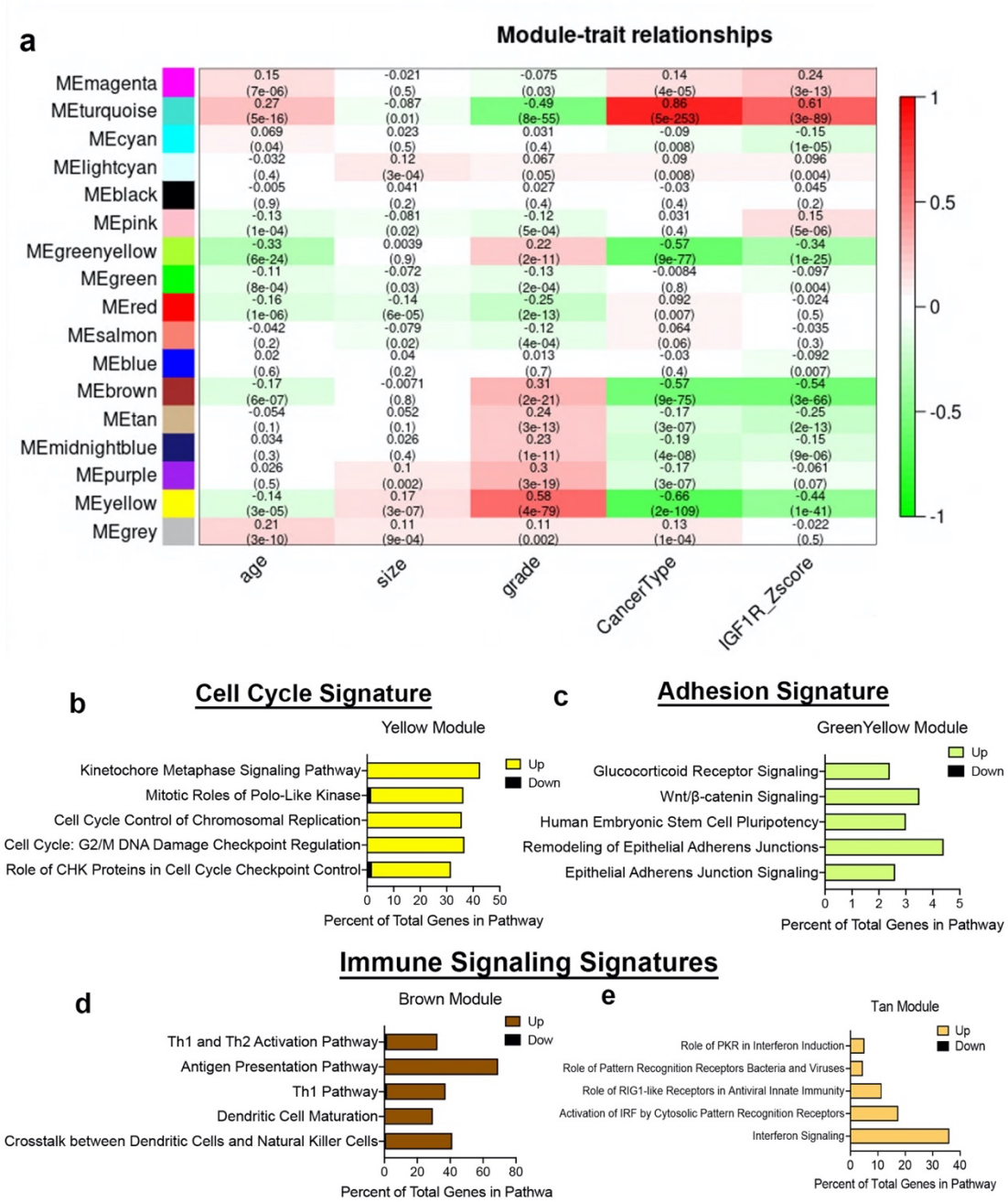


**Figure 1. Defining gene signatures associated with IGF-1R expression and tumor phenotype in human BCs. a.** Table of refined integrated WGCNA (IGF1R-GS2) showing module and clinical trait association. Each row corresponds to a module eigengene (ME), each column to a clinical measurement. Each cell contains the corresponding correlation and p- (in parentheses). The table is color-coded by correlation according to the color legend. Green < 0 for negative correlation; Red > 0, for positive correlation. **b-e.** Top 5 pathways identified by ingenuity pathway analysis (IPA) revealing key signatures in 4 modules inversely correlated with IGF-1R expression. (yellow module=cell cycle signature, greenyellow module=adhesion signature, brown and tan modules=immune signaling signatures).

213 Ingenuity pathway analysis (IPA) of IGF1R-GS2 for the pathways associated with
214 the lowest IGF-1R Z-scores revealed genes involved in control of cell cycle checkpoint
215 regulation and chromosome replication, (yellow, Cell Cycle Signature; Fig. 1b) and in
216 epithelial adherens junctions (green-yellow, Adhesion Signature; Fig. 1c). The two
217 additional modules associated with low IGF-1R contained genes involved in immune
218 cell signaling (brown, tan; Fig. 1d,e). Taken together, we hypothesize reduced IGF-1R
219 in breast tumors alters both intrinsic tumor epithelial cell pathways and extrinsic immune
220 microenvironment signatures to promote metastasis.
221 A major question that arises from the METABRIC WGCNA is whether there is a
222 causative relationship between IGF-1R expression and associated gene alterations and,
223 ultimately, phenotype of breast cancer. We published previously that low IGF-1R
224 expression predicts poor patient survival across all breast cancer subtypes (14, 23)
225 suggesting negative functional consequences from loss of IGF-1R expression. Our goal
226 in this study was to use mouse models to test the hypothesis from the human data that
227 low IGF-1R in breast tumors directly contributes to a metastatic phenotype through
228 dysregulated expression of specific cellular pathways.
229
230 *Mammary epithelial cell specific IGF-1R deletion promotes Wnt1 driven tumor*
231 *metastasis*
232 To test how loss of IGF-1R alters the primary tumor phenotype, we made use of
233 two distinct mouse models. In one model developed previously in our lab, IGF-1R
234 function is reduced through expression of a dominant-negative human *Igf1r* transgene

235 (*dnIgf1r*) in the *MMTV-Wnt1* (Wnt1) basal-like breast cancer tumor model (DN-Wnt1;
236 (23)). In this mouse line, the loss of IGF-1R function results in decreased tumor latency
237 and increased lung metastases, while tumor growth is unchanged (23). To model
238 human breast cancers with low IGF-1R expression, we also generated a mammary
239 luminal epithelial lineage-specific *Igf1r* knockout mouse driven from a tamoxifen-
240 inducible Keratin 8 (K8) promoter, referred to as the K8iKOR line (Fig. 2a; see Supp.
241 Methods). Loss of *Igf1r* was verified in mammary epithelial cells (MECs) isolated from
242 hyperplastic glands in 16-week-old virgin K8iKOR-Wnt1 mice compared to control, Wnt1
243 mice (Supp. Fig. 2a). Decreased *Igf1r* gene expression was maintained in tumors of the
244 K8iKOR-Wnt1 line (Supp. Fig. 2b).

245 To determine the effects of luminal epithelial specific *Igf1r* gene deletion in Wnt1-
246 driven mammary tumorigenesis, we assessed tumor latency rates in the K8iKOR-Wnt1
247 mouse line compared to the control Wnt1 line and to our prior tumor latency data on the
248 DN-Wnt1 mouse line (23). The mean tumor latency of Wnt1 mice was consistent with
249 previous reports (24, 25), where 50% of control Wnt1 animals formed palpable tumors
250 at 41.7 weeks of age (Fig. 2b). Tumor latency was significantly decreased in K8iKOR-
251 Wnt1 mice (12.5 weeks after tamoxifen injection, $p<0.0001$) (Fig. 2b) similar to the DN-
252 Wnt1 mouse line as previously reported (16.6 weeks, $p<0.0001$) (Fig. 2b) (23). Once
253 tumors formed, tumor growth was significantly increased in K8iKOR-Wnt1 compared to
254 control Wnt1 tumors (Fig. 2c). These data indicate that decreased expression of *Igf1r* in
255 luminal epithelial cells accelerates tumor initiation as well as tumor growth in the context
256 of elevated Wnt signaling.

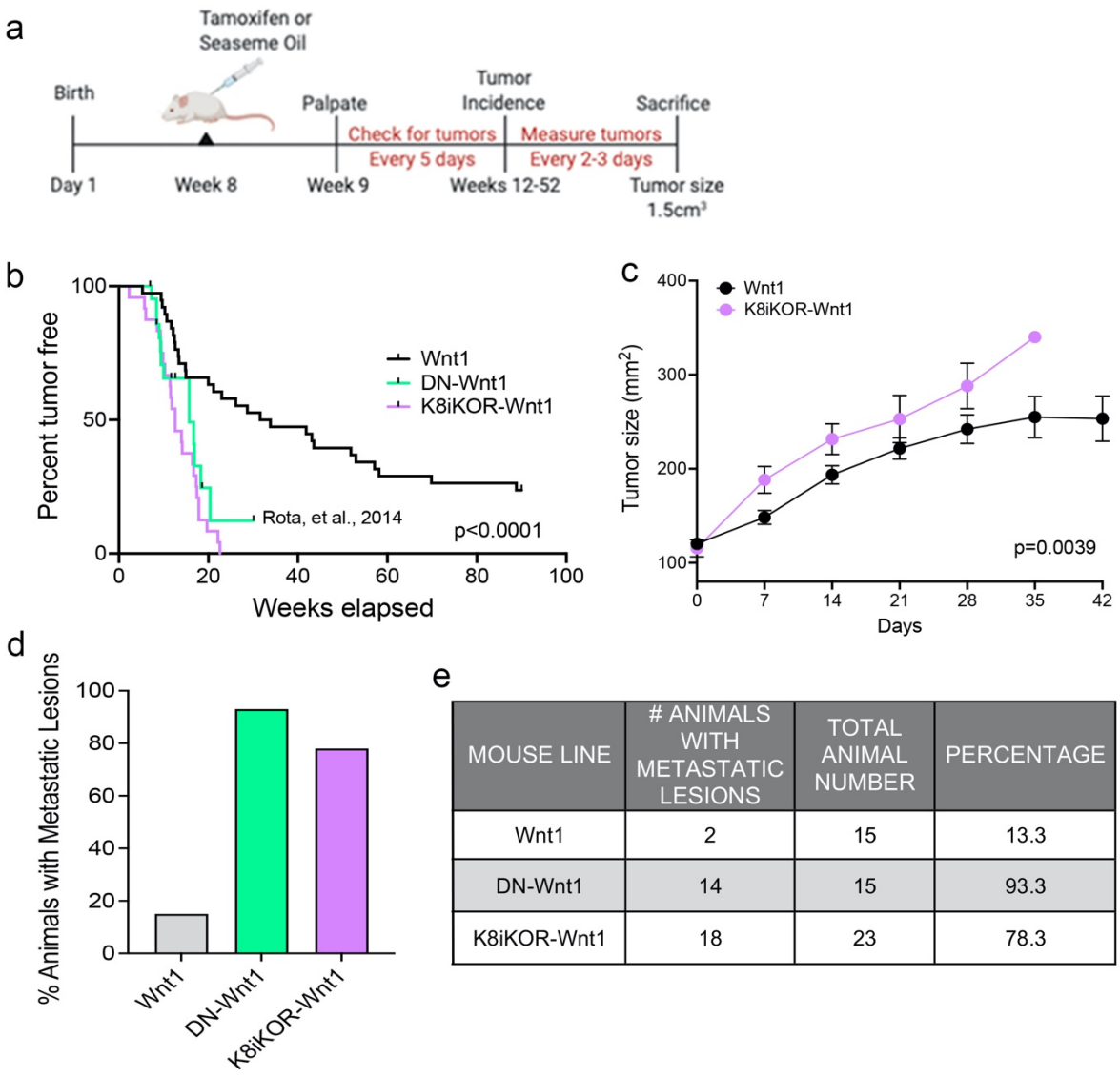


| MOUSE LINE | # ANIMALS WITH METASTATIC LESIONS | TOTAL ANIMAL NUMBER | PERCENTAGE |
|---|---|---|---|
| Wnt1 | 2 | 15 | 13.3 |
| DN-Wnt1 | 14 | 15 | 93.3 |
| K8iKOR-Wnt1 | 18 | 23 | 78.3 |

**Figure 2. Luminal loss of IGF-1R decreases tumor latency and increases metastasis. a.** Schematic for luminal lineage IGF-1R knockout. **b.** Latency curve for tumor development in Wnt1, DN-Wnt1, and K8iKOR-Wnt1 animals. For K8iKOR-Wnt1 animals, tumor latency is weeks post tamoxifen injection. *Statistic:* Mann-Whitney test **c.** Growth curve after tumors arise until time of euthanization. *Statistic:* Non-linear regression best fit for line slopes **d-e.** Graph of the percentage of animals **(d)** and table of number of animals **(e)** with metastatic lesions after establishment of a primary tumor. *Table Statistic*: Chi-square test; p=0.0251 for Wnt1 vs. DN-Wnt1 and K8iKOR-Wnt1. For Wnt1 controls, vehicle and tamoxifen injected animals were combined as the phenotypes were equivalent.

257 Although the Wnt1 tumors model a basal-like TNBC, these tumors have low
258 metastatic potential (24). In contrast, loss of luminal epithelial *Igf1r* in the Wnt1 tumors
259 significantly increased the percentage of animals with lung micrometastases similar to
260 the metastatic rate in the DN-Wnt1 mice (Fig. 2d,e). Thus, either reduced *Igf1r*
261 expression or reduced IGF-1R function in mammary epithelium promotes metastasis of
262 the primary Wnt1 tumor cells.
263
264 *Single-cell sequencing of mammary tumors to analyze epithelial IGF-1R function in*
265 *regulating tumor cell heterogeneity*
266 Reduced IGF-1R by function or by expression results in increased tumor
267 metastasis in the mouse models and aligns with human survival data indicating an
268 inverse relationship between IGF-1R expression and overall patient survival (14). The
269 mechanisms by which IGF-1R regulates tumor metastasis could include intrinsic
270 epithelial mesenchymal transition (EMT) changes as well as alterations to the tumor
271 microenvironment (TME) secondary to the genetic changes in the tumor epithelium. To
272 reveal underlying mechanisms and cell population changes downstream of alterations in
273 IGF-1R, we performed single cell RNA-sequencing (scRNA-seq) on the DN-Wnt1,
274 K8iKOR-Wnt1 and Wnt1 tumors. We initially analyzed scRNA-seq of the whole tumor to
275 profile changes in tumor cell populations when IGF-1R is either reduced or attenuated in
276 the tumor epithelium. Wnt1 control, DN-Wnt1 and K8iKOR-Wnt1 tumor cells were
277 plotted together resulting in 16 separate tumor cell populations (Fig. 3a). These
278 populations were further defined using cell specific markers resulting in the following

279 distinct cell populations: 6 epithelial, 2 fibroblast (CAF), 6 macrophage/monocyte
280 (MAC), 1 T-cell, and 1 endothelial (Fig. 3b,c, Supp. Fig. 3). Overall, loss of IGF-1R
281 expression or function resulted in decreased macrophage and T cell populations and
282 increased CAF populations (Fig. 3d). Ingenuity pathway analysis (IPA) supports the
283 conclusion that loss of IGF-1R function promotes an immune evasive TME (Fig. 3d,e,
284 Supp. Fig. 4). For example, while the cell number is unchanged in MAC Cluster 0 from
285 DN-Wnt1 and K8iKOR-Wnt1 tumors compared to Wnt1, the immune function pathways
286 are altered with downregulation of genes involved in immune cell activation, antigen
287 presentation, cell adhesion, and infiltration (Fig. 3e, Supp. Fig. 4a).
288 Alignment of the immune signature module from the METABRIC data analysis
289 (Fig. 1d) revealed several immune signaling pathways similarly associated with human
290 patient tumors with low IGF-1R expression and mouse tumors with reduced IGF-1R
291 function or expression (Fig. 3f). Interestingly, the pathways upregulated in both patient
292 and mouse tumors with reduced IGF-1R are important for response to stress signaling
293 and immune cell evasion supporting our prior findings that loss of IGF-1R promotes cell
294 stress in human breast cancer cells (14).
295
296 *Reduced IGF-1R alters the microenvironment to promote metastasis*
297 Our findings from the single cell analyses of the tumor modules suggest two
298 possible non-exclusive hypotheses: increased metastasis with decreased IGF-1R is due
299 to 1) microenvironment alterations, and/or 2) epithelial cell intrinsic alterations. To
300 directly test intrinsic tumor cell invasive capacity *in vivo* we performed tail vein injections

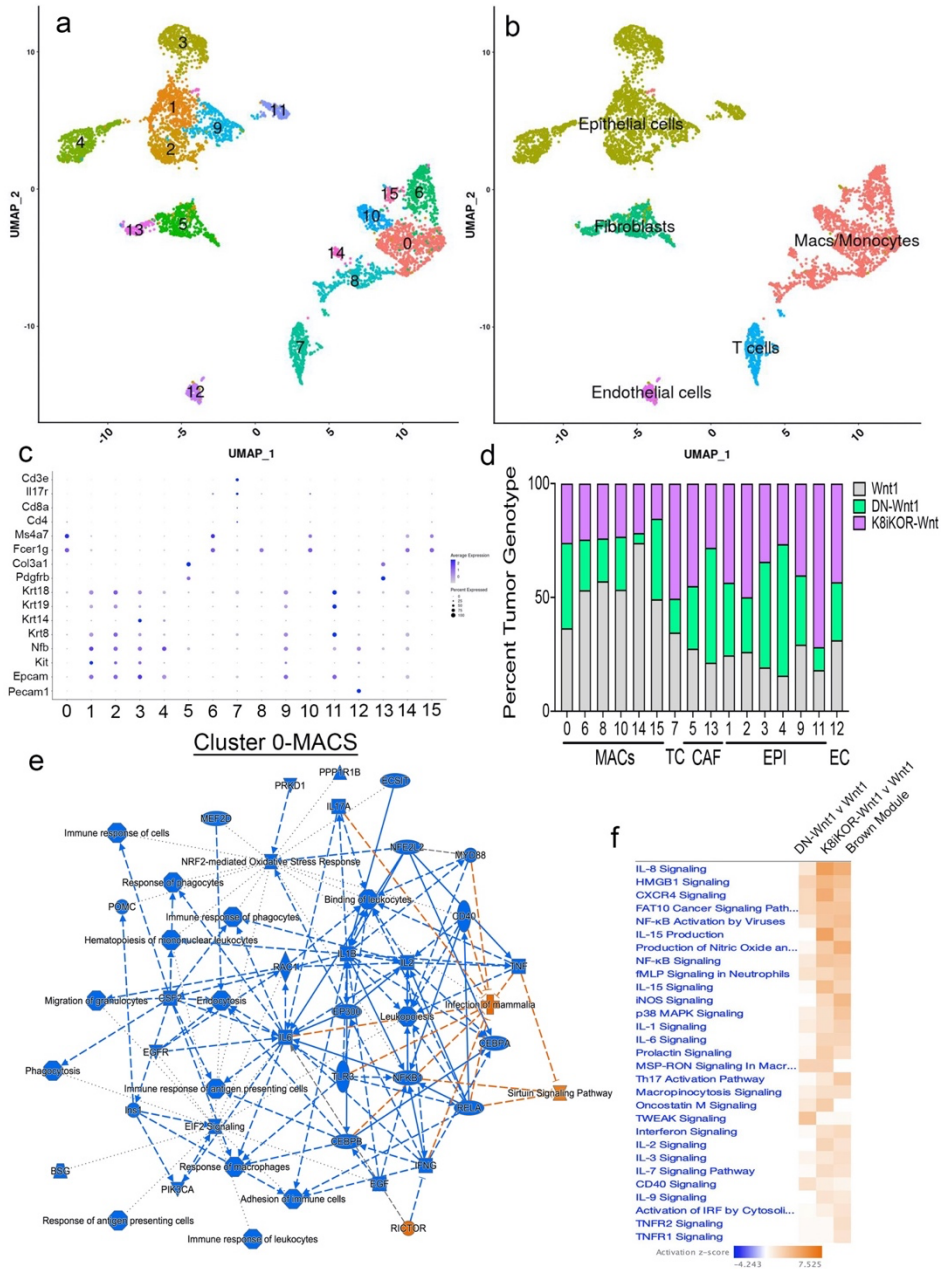


**Figure 3. Identifying mammary tumor heterogeneity by single cell RNA-sequencing. a.** Uniform Manifold Approximation and Projection (UMAP) plot of cells from Wnt1, DN-Wnt1, and K8iKOR-Wnt1 tumors resulting in 16 individual clusters. **b.** UMAP plot with identification of cluster cell types defined by known markers. **c.** Dot plot of cell markers. **d.** Percent tumor genotype graph for each cluster. Clusters are ordered by identified tumor cells. MAC and T-cell populations were generally decreased in DN-Wnt1 and K8iKOR-Wnt1 tumors. CAF populations were expanded in DN-Wnt1 and K8iKOR-Wnt1 tumors. (MACS=monocytes/macrophages, TC=T cells, CAF=fibroblasts, EPI=epithelial cells, EC=endothelial cells) **e.** IPA graphical summary of top pathway alterations in DN-Wnt1 compared to Wnt1 tumors from Cluster 0 (MACs). Blue=downregulated; orange=upregulated. **f.** IPA canonical pathways heat map of DN-Wnt1 and K8iKOR-Wnt1 compared to Wnt1 tumors and the METABRIC brown (immune signaling signature) module.

301 (TVI) with isolated tumor epithelial cells. We injected Wnt1, DN-Wnt1 or K8iKOR-Wnt1
302 tumor epithelial cells into tail veins of eGFP mice and analyzed lungs for metastases 1-
303 week post injection (1 wpi; Fig. 4a,b). Tumor cells from all three genotypes formed the
304 same number of micrometastases 1 wpi suggesting reduced IGF-1R does not alter the
305 epithelial cell invasive or seeding capacity (Fig. 4c). Furthermore, removing Wnt1 tumor
306 epithelial cells from the primary TME allows them to establish lung metastases
307 supporting the conclusion that intact IGF-1R signaling suppresses the ability of the
308 Wnt1 tumor epithelial cells to leave the primary tumor. Surprisingly, macrometastases
309 were only identified in the TVI lungs from Wnt1 and K8iKOR-Wnt1 tumor epithelial cells
310 (Fig. 4d). H&E-stained lung sections also showed significantly smaller micrometastases
311 in TVI lungs from DN-Wnt1 tumor epithelial cells 1 wpi (Fig. 4b).
312 The TVI results were surprising since the endogenous tumors that form in both
313 the DN-Wnt1 and K8iKOR-Wnt1 models lead to a high rate of metastasis. This suggests
314 that the process of dissociating the tumor epithelial cells alters the growth potential of
315 the DN-Wnt1 cells once the metastases have seeded. One possible explanation for the
316 discrepancy in lung metastatic growth after TVI between the two models is lineage
317 specificity of the IGF-1R disruption. The MMTV promoter is active early in the mammary
318 epithelial lineage such that both lineages express the transgene (26). RNAscope
319 immunofluorescence analysis for the human *dnIGF-1R* transgene confirmed expression
320 in hyperplastic mammary glands and tumors from the DN-Wnt1 mice (Supp. Fig. 5a-h)
321 as well as in micrometastases in TVI lungs from DN-Wnt1 tumor epithelial cells 1 wpi
322 and in endogenous primary micrometastases (Fig. 4e,f; Supp Fig. 5i-k). We then

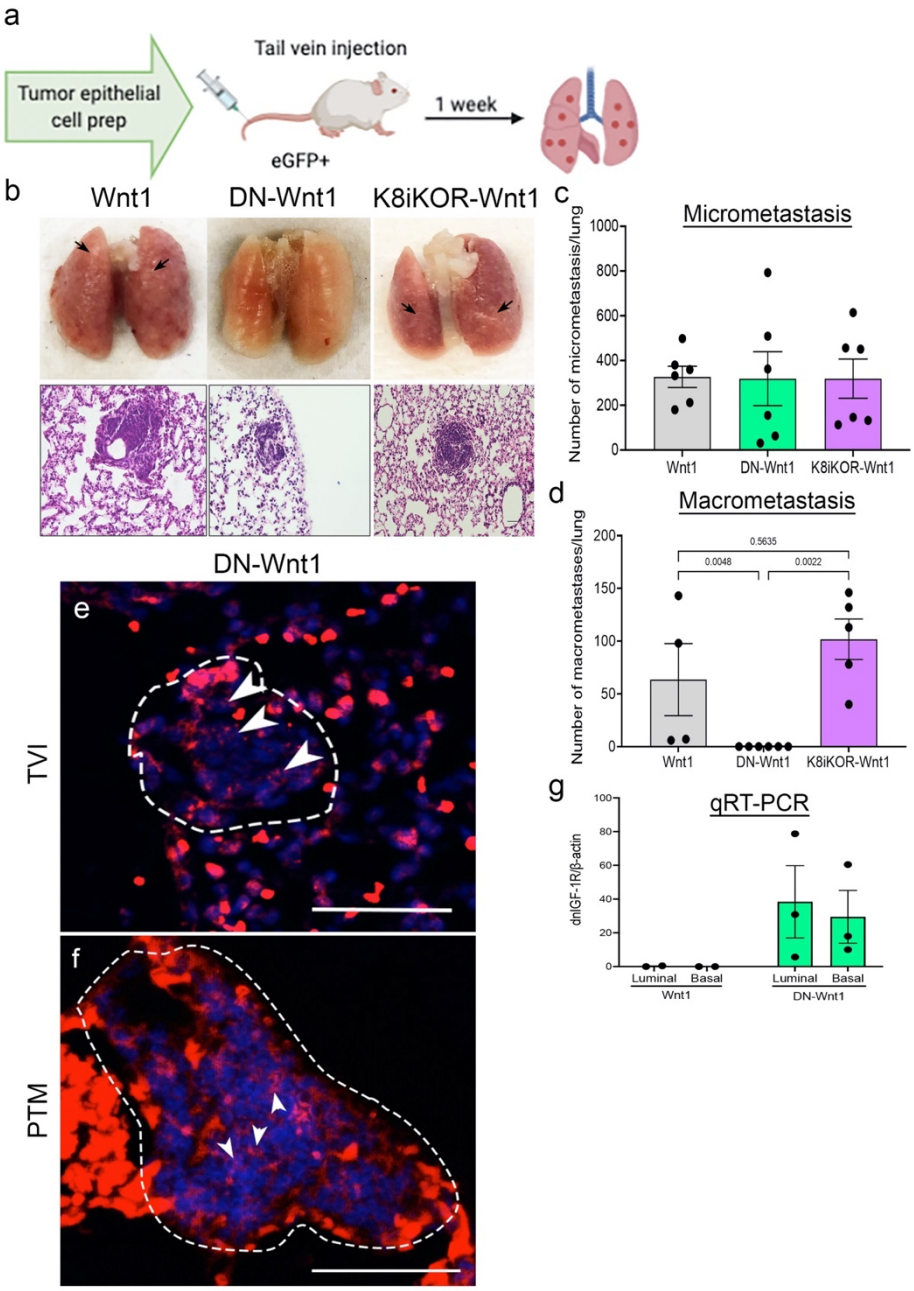


**Figure 4. Tail vein injections of primary tumor epithelial cells with reduced IGF-1R. a.** Schematic of tumor epithelial cell tail vein injection. **b.** Top Row: Representative whole lung images one-week after TVI of Wnt, DN-Wnt1, or K8iKOR-Wnt1 tumor epithelial cells. Arrows denote macroscopic metastases. Bottom Row: Representative lung hematoxylin and eosin staining for micrometastases from TVI of Wnt1, DN-Wnt1, or K8iKOR-Wnt1 tumor epithelial cells. Scale bar = 50 microns. **c-d.** Micrometastases **(c)** and macrometastases **(d)** counts from TVI lungs. *Statistic:* Non-parametric Kolmogorov Smirnov test **e-f.** RNAscope immunofluorescence for the human IGF-1R transgene (*dnIGF-1R*) in DN-Wnt1 TVI micrometastases 1 wpi **(e)** or in DN-Wnt1 endogenous primary tumor micrometastases (PTM) **(f)**. Scale bar = 50 microns **g.** RT-PCR for the human IGF-1R transgene in sorted primary tumor cells from Wnt1 and DN-Wnt1 tumors.

323 verified the expression of the *dnIGF-1R* transgene in both luminal and basal epithelial
324 lineages by performing qRT-PCR for the human *dnIGF-1R* transgene in tumor epithelial
325 cells following FACS (Fig. 4g). These findings support the hypothesis that the
326 differences in the TVI metastasis phenotype from the two IGF-1R models may be due to
327 disruption of IGF-1R in only the luminal lineage (K8iKOR-Wnt1) versus in both the
328 luminal and basal lineages (DN-Wnt1).
329
330 *Expansion of the metastatic tumor epithelial population with reduced IGF-1R*
331 We then asked 1) what are the cells from the DN-Wnt1 or K8iKOR-Wnt1 primary
332 tumors that seed lung metastases, 2) what properties of the epithelial cells from the DN-
333 Wnt1 tumor cells prevent their proliferation after TVI, and 3) why does luminal-specific
334 deletion of *Igf1r* maintain metastatic tumor growth after TVI? To address these
335 questions, we restricted the scRNA-Seq analysis to the tumor epithelial cell populations.
336 Unsupervised clustering using UMAP resulted in 13 distinct epithelial populations (E0-
337 E13) from 2,543 cells from Wnt1, DN-Wnt1, and K8iKOR-Wnt1 tumors (Fig. 5a). Using
338 Seurat analysis for keratin expression and heat map analysis of known epithelial cell
339 population markers (27) we identified the epithelial clusters as: alveolar (E0,E1), luminal
340 (E3,E4,E12), differentiated luminal (E6,E10), luminal progenitor (E2) and basal
341 (E5,E7,E8,E9,E11), one of which (E7) had high expression of the bipotential cell marker
342 Lgr5 (Fig. 5b-c, Supp. Fig. 6; see Supp. Methods). Importantly, 3 of the 5 differentiated
343 basal cell clusters (E5, E7, and E8) and the luminal progenitor cluster (E2) were
344 expanded in both the K8iKOR-Wnt1 and DN-Wnt1 tumors (Fig. 5d). The expansion of

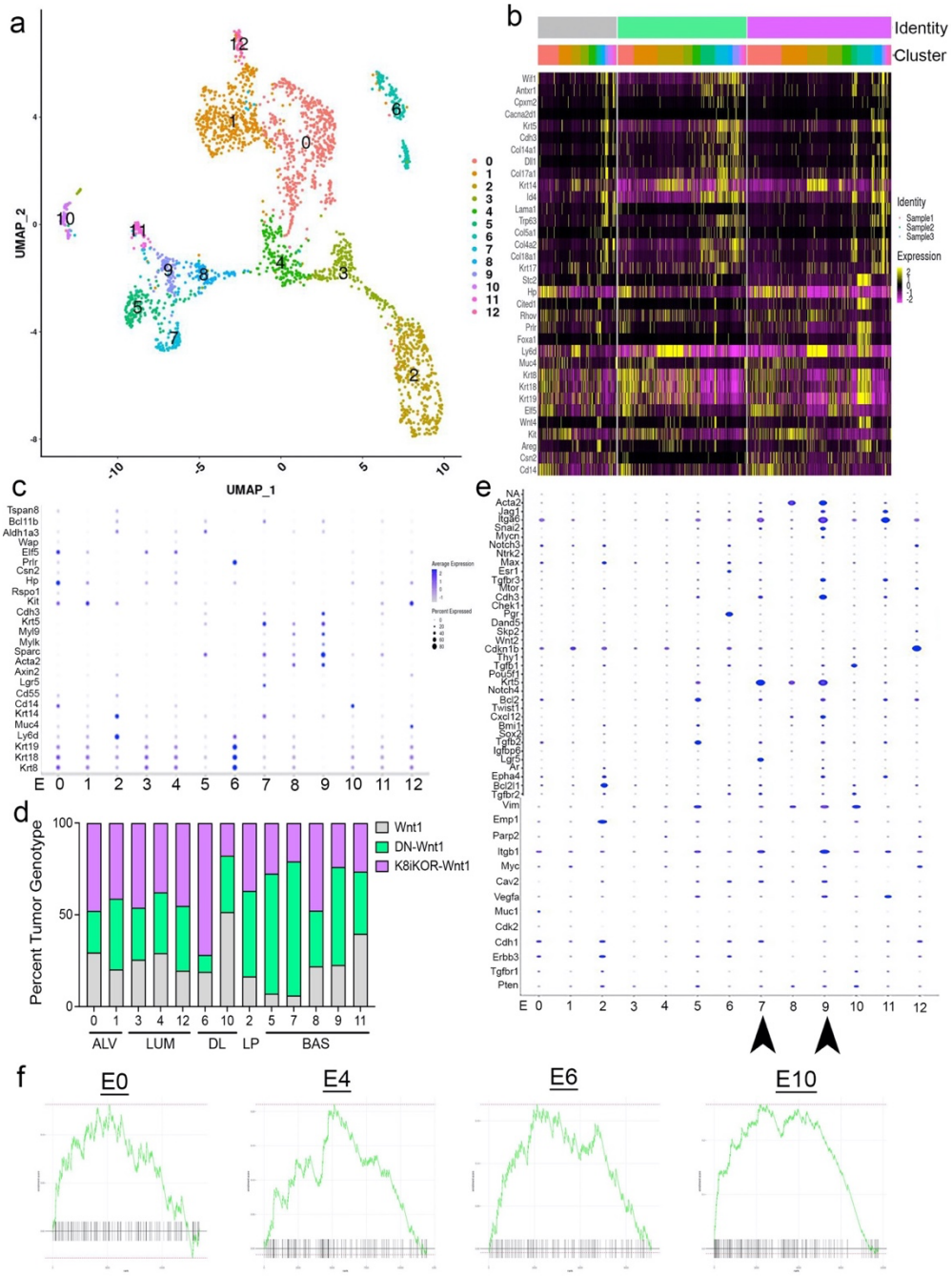


**Figure 5. Epithelial cell populations are altered with reduced IGF-1R. a.** UMAP plot of re-clustering of epithelial cells from Wnt1, DN-Wnt1, and K8iKOR-Wnt1 tumors resulting in 13 clusters. **b.** Heat map of top epithelial cell type markers. Top legend: top row=tumor identity: gray=Wnt1, green=DN-Wnt1, pink=K8iKOR-Wnt1; Bottom row=epithelial cell cluster. **c.** Dot plot of epithelial cell markers. **d.** Percent tumor genotype graph for each cell cluster labelled with each cell type defined by markers. (ALV=alveolar cell, LUM=luminal cell, DL=differentiated luminal cell, LP=luminal progenitor, BAS=basal cell) **e.** Dot plot of alignment with metastatic signature. Arrows depict clusters with high expression of markers indicating metastatic cell type. **f.** GSEA plots for the epithelial mesenchymal transition (EMT) hallmark signature in Clusters E0, E4, E6, and E10.

345 the basal and luminal progenitor populations in the DN-Wnt1 and K8iKOR-Wnt1 tumors
346 was supported by flow cytometry analyses (Supp. Fig. 7 and (23)).
347 Clusters E7 and E9 are most closely linked to a previously identified metastatic
348 signature (28) (Fig. 5e) consistent with increased metastasis in the IGF-1R deficient
349 tumor models (Fig. 2d,e). Gene Set Enrichment Analysis (GSEA) confirmed enrichment
350 in EMT (Fig. 5f; Supp. Fig. 8). IPA revealed key changes in cell migration and invasion
351 pathways specific to clusters E4, E5, E8, and E11 (Supp. Fig. 9). Increased EMT and
352 migration/invasion transcripts (Fig. 5b-e) suggests these populations are gaining
353 mesenchymal characteristics consistent with increased metastatic potential in both
354 basal and luminal populations in the IGF-1R deficient tumors.
355
356 *Attenuated IGF-1R decreases TVI metastatic growth by altering cell cycle*
357 We next asked what properties of the DN-Wnt1 cells resulted in the failure of the
358 micrometastases to proliferate and form macrometastasis in TVI mice. Analysis of lungs
359 from TVI mice past 1 wpi revealed decreased micrometastases in DN-Wnt1 TVI lungs
360 over time (Fig. 6b-c) suggesting maintenance of tumor epithelial cell proliferation and
361 survival is inhibited with attenuated IGF-1R when removed from the primary tumor niche
362 and dissociated prior to colonizing the lung. Furthermore, H&E staining revealed
363 maintenance of micrometastases at 3 and 6 wpi but degradation at 8 and 12 wpi (Fig.
364 6b). In contrast, lungs from TVI mice injected with either Wnt1 or K8iKOR-Wnt1 tumor
365 epithelial cells formed numerous macrometastases by 3 wpi (Fig. 6b).
366 To assess the role for IGF-1R in tumor epithelial cell proliferation we stained
367 tissue sections for phospho-histone H3 (pHH3). Interestingly, pHH3+ expression was

368 similar in hyperplastic glands and primary tumors from Wnt1, DN-Wnt1, and K8iKOR-
369 Wnt1 mice (Supp. Fig. 10). In contrast, pHH3 was undetectable at 1 wpi in TVI
370 micrometastases from DN-Wnt1 tumor epithelial cells but was detected in numerous
371 cells in TVI micrometastases from mice injected with Wnt1 and K8iKOR-Wnt1 tumor
372 epithelial cells (Fig. 6d). These data suggest that attenuation of IGF-1R inhibits
373 epithelial cell proliferation when cells are dissociated after removal from the primary
374 tumor niche. However, signature analysis by GSEA showed reduced enrichment for
375 genes associated with G2M checkpoint in clusters E7 and E10 and for genes
376 associated with mitotic spindle in clusters E1, E3 and E6 of the DN-Wnt1 vs Wnt1 tumor
377 cells (Fig. 6e) supporting alterations in proliferation in specific populations in the primary
378 tumor.
379 Comparison of the METABRIC cell cycle signature (Fig. 1b) with the whole
380 mouse tumor scRNA-seq transcripts revealed correlation of several cell cycle pathways
381 including cell cycle checkpoint, chromosome regulation, and apoptosis signaling further
382 supporting that loss of IGF-1R alters the cell cycle through changes in gene expression
383 (Fig. 6f).
384
385 *Collective metastatic seeding is diminished in tumor epithelial cells in DN-Wnt1 model*
386 The lack of proliferation in the DN-Wnt1 TVI metastases explains the observed
387 phenotype but does not explain the underlying reason for TVI metastases maintenance
388 and growth formed from K8iKOR-Wnt1 tumor cells. In addition to cell cycle changes in
389 the tumor epithelial cells with reduced IGF-1R, we also observe changes in pathways
390 involved in cell adhesion (Fig. 7). Several studies have reported collective cell invasion

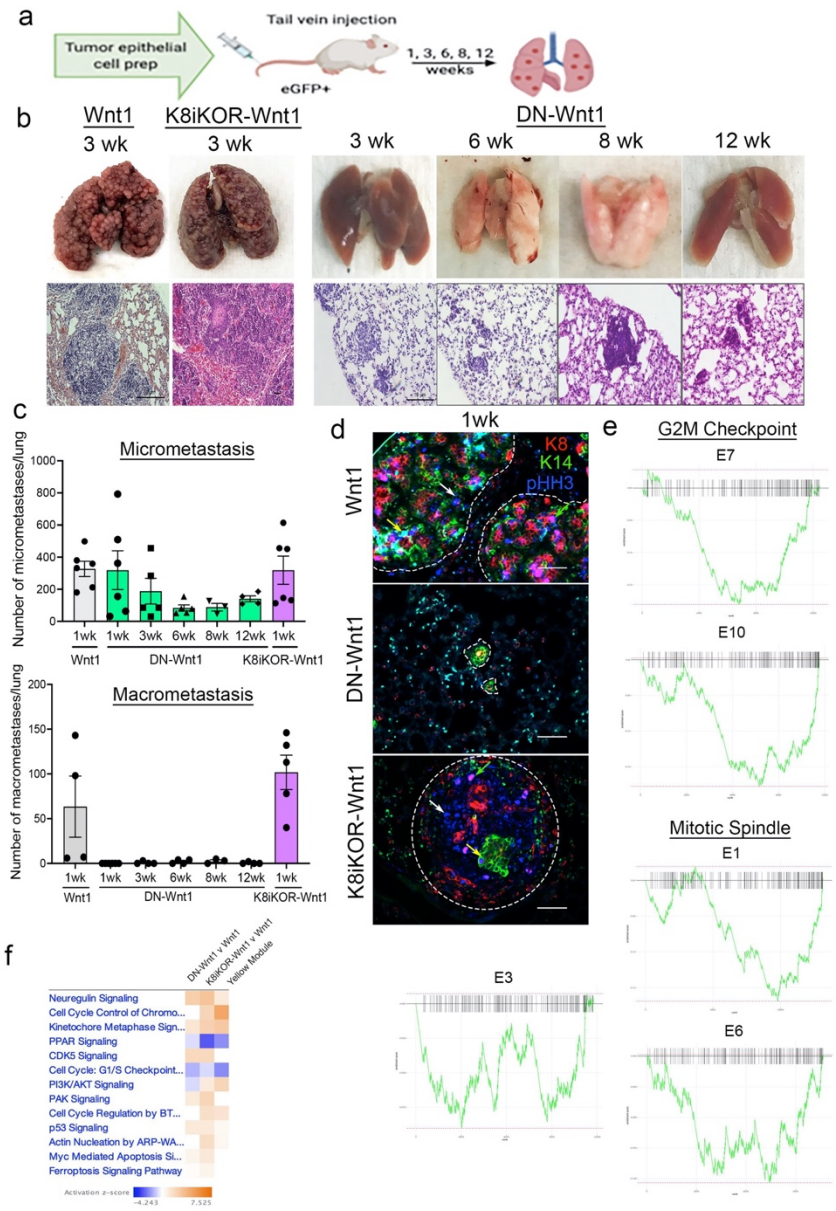


**Figure 6. Reduced IGF-1R reduces tumor cell growth and survival in lungs after tail vein injection. a.** Schematic of tumor epithelial cell tail vein injection. **b.** Top Row: Representative whole lung images after 3-, 6-, 8-, and 12-week TVI from Wnt1, DN-Wnt1, or K8iKOR-Wnt1 tumor epithelial cells. Bottom Row: Representative lung hematoxylin and eosin staining for micrometastases from TVI of Wnt1, DN-Wnt1, or K8iKOR-Wnt1 tumor epithelial cells over time. **c.** Micrometastases (top graph) and macrometastases (bottom graph) counts from TVI lungs over time. **d.** Immunofluorescence for K8 (red), K14 (green), and phospho-histone H3 (pHH3, blue) in metastases after 1wk TVI of Wnt1, DN-Wnt1, or K8iKOR-Wnt1 primary epithelial cells. Scale bar = 50 micron; representative of n=3. **e.** GSEA plots of G2M and Mitotic Spindle hallmark signatures in differentially expressed genes from DN-Wnt1 vs. Wnt1 epithelial cell clusters. **f.** IPA canonical pathway heat map of differentially expressed genes from DN-Wnt1 and K8iKOR-Wnt1 compared to Wnt1 tumors and the METABRIC (human) yellow (cell cycle) module.

391 is necessary to seed metastatic lesions and promote metastatic growth (29-31). This
392 invasion is dependent on K14$^+$ leader cells adhered to clusters of epithelial cells to
393 initiate collective invasion (29, 32). Micrometastases from TVI mice with either Wnt1 or
394 K8iKOR-Wnt1 tumor epithelial cells at 1 wpi were composed of K14$^+$ basal cells, K8$^+$
395 luminal cells, and a few K8$^+$/K14$^+$ double-positive cells (Fig. 7a-c). In contrast, lungs
396 from DN-Wnt1 TVI mice at 1 wpi were composed mostly of K14$^+$ leader cells (Fig. 7a-c).
397 These results suggest loss of IGF-1R expands the K14$^+$ leader cell population, but
398 phenotypic alterations within these cells decrease collective invasion to reduce
399 metastatic proliferation. One interesting question is which cell population(s) contribute to
400 the K14$^+$ leader cells. Previous reports have shown K8$^+$ luminal cells gain K14
401 expression and can also participate as metastatic, leader cells (29, 32). Both the DN-
402 Wnt1 and K8iKOR-Wnt1 tumors have increased basal cell populations (Fig. 5d);
403 however, we also found that sorted luminal cell populations from both tumors showed
404 increased expression of K14 compared to Wnt1 tumors (Fig. 7d). Thus, both basal and
405 luminal populations in tumors with reduced IGF-1R could be contributing K14$^+$ leader
406 cells to seed metastases.

407 *Cell adherence is altered in tumor epithelial cells with decreased IGF-1R function*

408 Smaller micrometastases composed of mostly K14$^+$ cells observed in the DN-
409 Wnt1 TVI lungs suggest a defect in adherence between the K14$^+$ leader cells and the
410 metastatic proliferating cells. Adherence was decreased in DN-Wnt1 and K8iKOR-Wnt1
411 compared to Wnt1 primary tumor epithelial cells in vitro (Fig. 7e). Consistent with these
412 findings, the number of DN-Wnt1 primary tumor epithelial cell clusters and single tumor

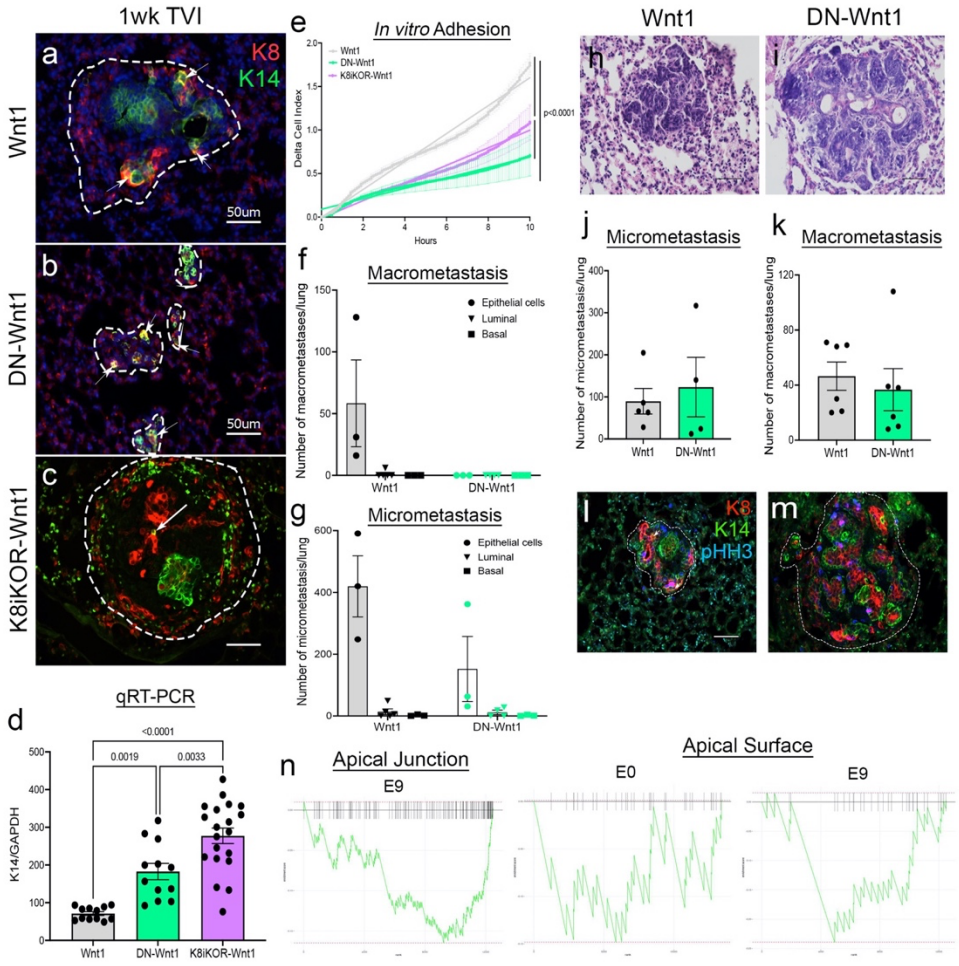


**Figure 7. Reduced IGF-1R function decreases tumor cell adhesion. a-c.** Representative TVI lung staining for K8 (red) and K14 (green) from Wnt1 **(a)**, DN-Wnt1 **(b)** and K8iKOR-Wnt1 **(c)** 1 wpi mice. Dotted lines demarcate the metastatic lesions. Arrows indicate double positive K8 and K14 cells. scale bar=50 micron; n=3. **d.** RT-PCR for K14 in sorted luminal ($CD24^{+}/CD29^{lo}$) primary tumor cells from Wnt1, DN-Wnt1, and K8iKOR-Wnt1 tumors showing increased expression in both IGF-1R models. *Statistic:* Mann-Whitney U non-parametric t test. **e.** Measurement of adhesion from Wnt1 (grey), DN-Wnt1 (green), or K8iKOR-Wnt1 (purple) by delta cell index over time for 6 hours using the real-time xCELLigence assay. n=3; *Statistic:* Non-linear regression least squares regression for slope best fit $p<0.0001$ for Wnt1 control compared to DN-Wnt1 or K8iKOR-Wnt1 **f-g.** Macrometastases **(f)** or micrometastases **(g)** counts in lungs from TVI mice injected with Wnt1 or DN-Wnt1 tumor epithelial cells (250K), sorted luminal epithelial cells, or sorted basal epithelial cells after 1 wpi. **h-i.** Representative H&E images from Wnt1 **(h)** and DN-Wnt1 **(i)** lung micrometastases from TVI mice injected with Wnt1 or DN-Wnt1 tumor epithelial cells cultured overnight at low adherence. **j-k.** Micrometastases **(j)** and macrometastases **(k)** counts in lungs from TVI mice injected with Wnt1 or DN-Wnt1 tumor epithelial cells cultured overnight at low adherence. **l-m.** Immunofluorescence of K8 (red), K14 (green), and pHH3 (blue) in Wnt1 **(l)** and DN-Wnt1 **(m)** TVI micrometastases from tumor epithelial cells cultured overnight at low adherence. **n.** GSEA plots for the apical junction and apical surface hallmark signatures from differentially expressed genes in DN-Wnt1 vs. Wnt1 epithelial tumor cell clusters.

413 epithelial cells had decreased adherence to collagen matrix compared to Wnt1 primary
414 tumor cells (Supp. Fig. 11a-e). In contrast, there was no significant difference between
415 the K8iKOR-Wnt1 and Wnt1 primary tumor epithelial cells in their ability to adhere to
416 collagen (Supp. Fig. 11a-e). Immunofluorescence revealed increased $K14^+$ and
417 decreased K8+ cell adherence from DN-Wnt1 compared to Wnt1 primary tumors both in
418 clusters and individual cells (Supp. Fig.11f,g) consistent with *in vivo* TVI analysis (Fig.
419 7a-c). Moreover, the non-adherent cells from the DN-Wnt1 tumors had increased E-
420 cadherin and cyclin D1 expression indicating these are the proliferating luminal
421 epithelial cells (Supp. Fig. 11h,i). Taken together, these data support the conclusion that
422 attenuated IGF-1R with the *dnIGF-1R* transgene alters adherence between the $K14^+$
423 leader cell and other epithelial cells, particularly those that are necessary to proliferate
424 in the metastatic lesion, while deletion of luminal *Igf1r* does not alter adherence to the
425 same extent. These findings support the hypothesis that disruption of IGF-1R in both
426 the luminal and basal lineages in the DN-Wnt1 tumors (Fig. 4) is necessary to disrupt
427 adhesion between epithelial cells.

428 Our data and other recent studies (33-36) indicate that cell adherence is
429 necessary to promote metastatic seeding and growth. We next asked whether paracrine
430 signaling between the epithelial cell populations is necessary to maintain metastatic
431 growth. Primary tumor epithelial cells from Wnt1 or DN-Wnt1 mice were sorted for
432 luminal ($CD24^+/CD29^{lo}$) and basal ($CD24^+/CD29^{hi}$) epithelial populations and injected
433 into the tail vein of eGFP mice. Importantly, lung macrometastases were significantly
434 decreased in the sorted populations from Wnt1 tumor compared to combined epithelial

435 cell TVIs (Fig. 7f). Similarly, we observed decreased lung micrometastases from both
436 Wnt1 and DN-Wnt1 sorted population TVIs compared to combined epithelial cells (Fig.
437 7g). These data support the conclusion that luminal and basal epithelial cell adherence
438 is necessary for metastatic seeding and growth.

439 To test whether restoration of lineage associations would restore metastatic
440 growth in the DN-Wnt1 tumor cells, we performed TVIs with primary epithelial cells from
441 Wnt1 or DN-Wnt1 tumors cultured overnight in low adherent plates to allow for cell re-
442 adherence after dissociation. Enhancing cell adhesion by overnight incubation resulted
443 in similar numbers of macrometastases and micrometastases in DN-Wnt1 and Wnt1
444 TVI primary tumor epithelial cells (Fig. 7h-k). Further analysis by immunofluorescence
445 revealed pHH3$^+$ and K8$^+$ micrometastases from DN-Wnt1 epithelial cells 1 wpi similar to
446 Wnt1 micrometastases (Fig. 5, Fig. 7l,m) suggesting decreased cell adherence in DN-
447 Wnt1 tumor epithelial cells is amplified by tumor dissociation. Analysis of adhesion
448 target transcripts identified upregulation of adhesion in Cluster E2 (luminal progenitor)
449 across all tumor types and downregulation of adhesion in the basal cell clusters
450 (Clusters E5, E7, E8, and E9) in DN-Wnt1 tumors (Fig. 7n, Supp. Fig 12a).

451

452 *Cell adherence is dysregulated by enhanced P-cadherin expression in epithelial cells*
453 *with reduced IGF-1R function*

454 Recently, the Ewald lab reported E-cadherin loss is required for metastatic
455 invasion, and its re-expression is necessary to promote metastatic growth (37).
456 Furthermore, upregulation of P-cadherin and its co-expression with E-cadherin in the

457 primary tumor is a marker of more aggressive, metastatic breast tumors (38-41). To
458 determine if cadherin expression changes with IGF-1R expression in patient tumors, we
459 analyzed the METABRIC dataset and identified an inverse correlation of P-cadherin and
460 IGF-1R expression. Conversely, E-cadherin is positively correlated with IGF-1R
461 expression across all breast tumors (Fig. 8a).

462 To determine whether cadherin expression is similarly altered in the DN-Wnt1
463 tumors, we screened for cadherin expression in each epithelial cluster from the scRNA-
464 Seq data. As expected, luminal cell types had higher E-cadherin (Cdh1) expression
465 whereas basal cell types had higher P-cadherin (Cdh3) and T-cadherin (Cdh13)
466 expression (Supp. Fig. 12b). E-cadherin expression in DN-Wnt1 tumor epithelial cells by
467 qRT-PCR was decreased compared to Wnt1 cells (Supp. Fig. 12c). Moreover, E-
468 cadherin levels were decreased in clusters E5 and E7 (Fig. 8b), which also expressed
469 P-cadherin (Fig. 8c). Immunostaining similarly showed decreased E-cadherin and
470 increased P-cadherin protein expression in DN-Wnt1 and K8iKOR-Wnt1 primary tumors
471 compared to Wnt1 tumors (Fig. 8d-m). Interestingly, total E-cadherin expression was
472 altered primarily at the protein level, while P-cadherin was changed at both the RNA
473 and protein levels in tumors with reduced IGF-1R. Importantly, co-expression of E-
474 cadherin and P-cadherin was increased in DN-Wnt1 and K8iKOR-Wnt1 tumors (Fig. 8d-
475 m). Thus, reduced IGF-1R was associated with altered E-cadherin and P-cadherin in
476 tumor epithelial cells.

477 To test the functional role of altered E-cadherin and P-cadherin in cells with
478 attenuated IGF-1R, we first transiently re-expressed E-cadherin in DN-Wnt1 primary

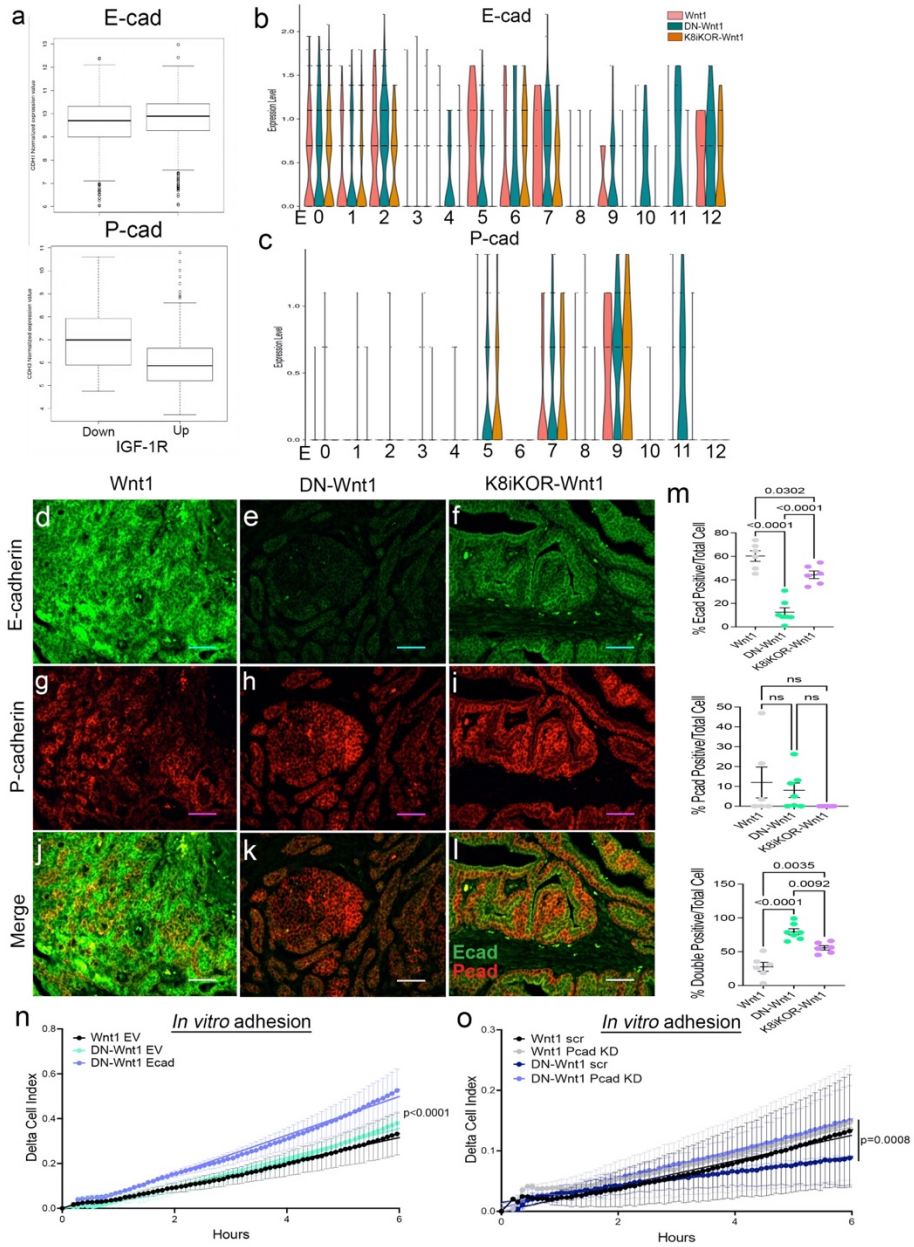


**Figure 8. Altered cadherin expression in tumors with reduced IGF-1R. a.** METABRIC data analysis for E-cadherin or P-cadherin in patient tumors with low IGF-1R (IGF-1R z-score < -1) or high IGF-1R (IGF-1R z-score > 1) ($p < 2.0x10^{-16}$) *Statistic:* Student's *t*-test. **b-c.** E-cadherin **(b)** and P-cadherin **(c)** expression in each epithelial cell cluster identified with single-cell sequencing in Wnt1, DN-Wnt1, or K8iKOR-Wnt1 primary tumors. **d-m.** Representative images of E-cadherin (red) or P-cadherin (green) immunostaining in Wnt1 **(d, g, j)**, DN-Wnt1 **(e, h, k)**, and K8iKOR-Wnt1 **(f, i, l)** primary tumors. **m.** E-cadherin, P-cadherin, and double positive cell count graphs of primary tumors. *Statistic:* One-Way ANOVA with Tukey's Multiple Comparison post-hoc test **n.** Adhesion (delta cell index) over time in Wnt1 or DN-Wnt1 primary tumors with empty vector (EV) or E-cadherin overexpression (Ecad). n=3; *Statistic:* Non-linear regression. **o.** Adhesion (delta cell index) over time in Wnt1 or DN-Wnt1 with P-cadherin knockdown (Pcad KD). n=3; *Statistic:* Non-linear regression.

479 tumor epithelial cells and measured cell adhesion *in vitro*. Overexpression of E-cadherin
480 increased epithelial cell adhesion compared to empty vector control (Fig. 8n).
481 Furthermore, reducing P-cadherin in DNA-Wnt1 primary tumor epithelial cells
482 significantly increased tumor adhesion restoring adhesion back to the level of the Wnt1
483 tumor cells (Fig. 8o). Thus, altering cadherins in DN-Wnt1 primary tumor epithelial cells
484 rescues the compromised adherence suggesting these changes in E- and P-cadherins
485 due to reduced IGF-1R are necessary for metastasis.
486

487 **Discussion**

488 A major question in cancer biology is how do primary tumor cells metastasize to
489 another site? Here we show loss of IGF-1R in the primary tumor promotes metastasis
490 by modulating cadherin expression, altering epithelial cell properties and increasing
491 basal leader cells for collective invasion. Furthermore, reduced IGF-1R function or
492 expression increases metastatic extravasation. Surprisingly, once the primary tumor
493 cells are removed from the tumor niche and dissociated we discovered loss of IGF-1R
494 function promotes tumor cell quiescence.

495 While it is well established that epithelial cells gain mesenchymal cell properties
496 to migrate out of the primary tumor (29-32, 36), several recent studies have shown only
497 a subset of mesenchymal properties are necessary for migration and invasion referred
498 to as partial EMT (42-45). While original dogma was that the metastatic process occurs
499 by single tumor epithelial cell migration and invasion, recent observations of collective
500 epithelial cell migration have presented a new mechanism for metastasis that relies on

501 interactions between a mesenchymal-like leader cell with other epithelial cells in the
502 primary tumor (36). Thus, understanding how cell-cell interactions are regulated both in
503 the primary tumor and at distant sites of colonization is critical to determining metastatic
504 potential of tumor cells.

505 Loss of E-cadherin is a hallmark of EMT and necessary for basal cells to adapt to
506 becoming leader metastatic cells (29). The Ewald lab previously described a process by
507 which the transition of E-cadherin expression is critical for collective invasion (37). Here,
508 we have shown E-cadherin expression is decreased in mouse models with reduced
509 function or expression of IGF-1R to drive collective invasion. In the TVI models, we
510 show that loss of adhesion between epithelial cells compromises collective invasion to
511 promote growth of the metastatic lesions. Interestingly, recent reports have shown
512 acquisition of P-cadherin is necessary for tumor cells to become metastatic. More
513 importantly, the co-expression of P-cadherin and E-cadherin is critical for enhanced
514 metastasis and suggests these cells are exhibiting a partial EMT phenotype.
515 Attenuation or reduced IGF-1R levels in the Wnt1 mouse tumor model results in co-
516 expression of P-cadherin and E-cadherin and a partial EMT phenotype suggesting
517 increased metastatic properties of these tumor cells.

518 While loss of IGF-1R is sufficient to drive a partial EMT phenotype and collective
519 invasion to promote metastasis, alterations in the tumor microenvironment may also be
520 required for increased tumor extravasation. Our previous studies showed heightened
521 cell stress driven by attenuated IGF-1R resulted in immune cell evasion and a pro-
522 metastatic tumor microenvironment (14). Furthermore, the TVI model demonstrated that

523 removing the Wnt1 tumor cells from their primary microenvironment was sufficient to
524 promote their metastasis after TVI suggesting alterations in the TME driven by
525 attenuating IGF-1R promote metastasis.

526 While a similar metastatic process is observed in the DN-Wnt1 and K8iKOR-
527 Wnt1 primary tumor models, the TVI experiments revealed clear differences in the
528 phenotype of the primary tumor cells in these models. There are two key differences in
529 these models that likely contribute to these findings: 1) the DN-Wnt1 model attenuates
530 the receptor activity whereas the K8iKOR-Wnt1 model is a gene knockout in the luminal
531 epithelium, and 2) the *dnIGF-1R* transgene is expressed in luminal and basal epithelial
532 cells blocking the receptor function in all mammary epithelium, whereas receptor
533 expression is decreased only in the luminal epithelial cells in the K8iKOR-Wnt1 model
534 leaving the basal cell IGF-1R intact. Potentially, the loss of IGF-1R function in both
535 luminal and basal epithelial cells may lead to the observed TVI model phenotype
536 because of reduced adherence. These findings emphasize modeling importance.

537 It is clear from the spontaneous tumor models attenuated or loss of IGF-1R
538 decreases tumor latency and increases metastasis. These results are consistent with
539 the clinical data where trials inhibiting IGF-1R have been unsuccessful. The
540 interconnectedness of the tumor epithelium and microenvironment is highly complex.
541 The advantage of our models is the ability to study stochastic tumor progression in the
542 context of the microenvironment which reveals this complex tumor biology. Importantly,
543 the mouse modeling data aligns with the human gene expression and pathway analyses

544 and provides a basis for understanding why loss of IGF-1R in human breast cancers is
545 associated with a worse outcome.
546
547 **Data Availability Statement**
548 The data generated in this study will be made publicly available upon publication.
549
550 **Acknowledgements**
551 This work was supported by Public Health Service National Institutes of Health grants
552 NCI R01CA204312 (T.L.W) and NCI R01CA128799 (D.L.), New Jersey Commission on
553 Cancer Research Postdoctoral Fellowship DFHS15PPC039 and American Cancer
554 Society-Fairfield County Roast Postdoctoral Fellowship 130455-PF-17-244-01-CSM
555 (A.E.O.). We thank Dr. Sukhwinder Singh of the NJMS Flow Cytometry and
556 Immunology Core Laboratory for the assistance with flow cytometry analysis and
557 sorting, the Office of Advanced Research Computing (OARC) at Rutgers
558 University under NIH 1S10OD012346-01A1 for the critical work made possible through
559 access to the Perceval Linux cluster, BioRender.com for access to create the graphical
560 abstract, and Dr. Yi Li for providing the *MMTV-Wnt1* mice.
561
562 **Author contributions**
563 AEO performed the majority of the experiments and statistical analyses, participated in
564 the study design and wrote the manuscript. Y-JC performed the WGCNA METABRIC
565 analysis. VC performed the initial analyses on the K8iKOR-Wnt1 mouse tumor line. AL
566 performed the scRNA-Seq analyses. KM performed metastases quantification,

567 RNAScope and participated in the *in vitro* adhesion assays and study design. JJB
568 performed metastases quantification, qRT-PCR for *Igf1r* deletion in sorted cell
569 populations and participated in the *in vitro* adhesion assays and study design. QS
570 performed mouse genotyping, tamoxifen tests, gland analyses and tumor harvesting.
571 EG and DL contributed to results interpretation and manuscript editing. TLW is the
572 principal investigator for this project and was involved in study design, data analysis,
573 manuscript editing and submission. All authors read and approved the final manuscript.
574

575 **Competing interests**

576 The authors declare no competing interests.

577

578 References
579
580 1. Lero MW, Shaw LM. Diversity of insulin and IGF signaling in breast cancer:
581 Implications for therapy. Mol Cell Endocrinol. 2021;527:111213.
582 2. Ali R, Wendt MK. The paradoxical functions of EGFR during breast cancer
583 progression. Signal Transduct Target Ther. 2017;2.
584 3. Carvalho I, Milanezi F, Martins A, Reis RM, Schmitt F. Overexpression of
585 platelet-derived growth factor receptor alpha in breast cancer is associated with tumour
586 progression. Breast Cancer Res. 2005;7(5):R788-95.
587 4. Nassar A, Khoor A, Radhakrishnan R, Radhakrishnan A, Cohen C. Correlation of
588 HER2 overexpression with gene amplification and its relation to chromosome 17
589 aneuploidy: a 5-year experience with invasive ductal and lobular carcinomas. Int J Clin
590 Exp Pathol. 2014;7(9):6254-61.
591 5. Yang Y, Yee D. Targeting insulin and insulin-like growth factor signaling in breast
592 cancer. J Mammary Gland Biol Neoplasia. 2012;17(3-4):251-61.
593 6. Boone DN, Lee AV. Targeting the insulin-like growth factor receptor: developing
594 biomarkers from gene expression profiling. Critical reviews in oncogenesis.
595 2012;17(2):161-73.
596 7. Pollak M. Insulin and insulin-like growth factor signalling in neoplasia. Nat Rev
597 Cancer. 2008;8(12):915-28.
598 8. Belfiore A, Frasca F. IGF and insulin receptor signaling in breast cancer. J
599 Mammary Gland Biol Neoplasia. 2008;13(4):381-406.
600 9. Lann D, LeRoith D. The role of endocrine insulin-like growth factor-I and insulin in
601 breast cancer. J Mammary Gland Biol Neoplasia. 2008;13(4):371-9.
602 10. Papa V, Gliozzo B, Clark GM, McGuire WL, Moore D, Fujita-Yamaguchi Y, et al.
603 Insulin-like growth factor-I receptors are overexpressed and predict a low risk in human
604 breast cancer. Cancer Res. 1993;53(16):3736-40.
605 11. Bonneterre J, Peyrat JP, Beuscart R, Demaille A. Prognostic significance of
606 insulin-like growth factor 1 receptors in human breast cancer. Cancer Res.
607 1990;50(21):6931-5.

608 12. Yerushalmi R, Gelmon KA, Leung S, Gao D, Cheang M, Pollak M, et al. Insulin-
609 like growth factor receptor (IGF-1R) in breast cancer subtypes. Breast Cancer Res
610 Treat. 2012;132(1):131-42.
611 13. Farabaugh SM, Chan BT, Cui X, Dearth RK, Lee AV. Lack of interaction between
612 ErbB2 and insulin receptor substrate signaling in breast cancer. Cell Commun Signal.
613 2016;14(1):25.
614 14. Obr AE, Kumar S, Chang YJ, Bulatowicz JJ, Barnes BJ, Birge RB, et al. Insulin-
615 like growth factor receptor signaling in breast tumor epithelium protects cells from
616 endoplasmic reticulum stress and regulates the tumor microenvironment. Breast Cancer
617 Res. 2018;20(1):138.
618 15. Rota LM, Albanito L, Shin ME, Goyeneche CL, Shushanov S, Gallagher EJ, et al.
619 IGF1R inhibition in mammary epithelia promotes canonical Wnt signaling and Wnt1-
620 driven tumors. Cancer research. 2014;74(19):5668-79.
621 16. Cadoret A, Desbois-Mouthon C, Wendum D, Leneuve P, Perret C, Tronche F, et
622 al. c-myc-induced hepatocarcinogenesis in the absence of IGF-I receptor. Int J Cancer.
623 2005;114(4):668-72.
624 17. Van Keymeulen A, Rocha AS, Ousset M, Beck B, Bouvencourt G, Rock J, et al.
625 Distinct stem cells contribute to mammary gland development and maintenance.
626 Nature. 2011;479(7372):189-93.
627 18. Muller PY, Janovjak H, Miserez AR, Dobbie Z. Processing of gene expression
628 data generated by quantitative real-time RT-PCR. Biotechniques. 2002;32(6):1372-4, 6,
629 8-9.
630 19. Sun Z, Shushanov S, Leroith D, Wood TL. Decreased IGF Type 1 Receptor
631 Signaling in Mammary Epithelium during Pregnancy Leads to Reduced Proliferation,
632 Alveolar Differentiation, and Expression of Insulin Receptor Substrate (IRS)-1 and IRS-
633 2. Endocrinology. 2011;152(8):3233-45.
634 20. Obr AE, Grimm SL, Bishop KA, Pike JW, Lydon JP, Edwards DP. Progesterone
635 receptor and Stat5 signaling cross talk through RANKL in mammary epithelial cells. Mol
636 Endocrinol. 2013;27(11):1808-24.

637 21. Curtis C, Shah SP, Chin SF, Turashvili G, Rueda OM, Dunning MJ, et al. The
638 genomic and transcriptomic architecture of 2,000 breast tumours reveals novel
639 subgroups. Nature. 2012;486(7403):346-52.
640 22. Fu P, Ibusuki M, Yamamoto Y, Hayashi M, Murakami K, Zheng S, et al. Insulin-
641 like growth factor-1 receptor gene expression is associated with survival in breast
642 cancer: a comprehensive analysis of gene copy number, mRNA and protein expression.
643 Breast cancer research and treatment. 2011;130(1):307-17.
644 23. Rota LM, Albanito L, Shin ME, Goyeneche CL, Shushanov S, Gallagher EJ, et al.
645 IGF1R Inhibition in Mammary Epithelia Promotes Canonical Wnt Signaling and Wnt1-
646 Driven Tumors. Cancer Res. 2014;74(19):1-12.
647 24. Li Y, Hively WP, Varmus HE. Use of MMTV-Wnt-1 transgenic mice for studying
648 the genetic basis of breast cancer. Oncogene. 2000;19(8):1002-9.
649 25. Pond AC, Herschkowitz JI, Schwertfeger KL, Welm B, Zhang Y, York B, et al.
650 Fibroblast growth factor receptor signaling dramatically accelerates tumorigenesis and
651 enhances oncoprotein translation in the mouse mammary tumor virus-Wnt-1 mouse
652 model of breast cancer. Cancer Res. 2010;70(12):4868-79.
653 26. Wagner KU, McAllister K, Ward T, Davis B, Wiseman R, Hennighausen L.
654 Spatial and temporal expression of the Cre gene under the control of the MMTV-LTR in
655 different lines of transgenic mice. Transgenic Res. 2001;10(6):545-53.
656 27. Visvader JE, Stingl J. Mammary stem cells and the differentiation hierarchy:
657 current status and perspectives. Genes Dev. 2014;28(11):1143-58.
658 28. Davis RT, Blake K, Ma D, Gabra MBI, Hernandez GA, Phung AT, et al.
659 Transcriptional diversity and bioenergetic shift in human breast cancer metastasis
660 revealed by single-cell RNA sequencing. Nat Cell Biol. 2020;22(3):310-20.
661 29. Cheung KJ, Gabrielson E, Werb Z, Ewald AJ. Collective invasion in breast
662 cancer requires a conserved basal epithelial program. Cell. 2013;155(7):1639-51.
663 30. Khalil AA, Ilina O, Gritsenko PG, Bult P, Span PN, Friedl P. Collective invasion in
664 ductal and lobular breast cancer associates with distant metastasis. Clin Exp
665 Metastasis. 2017;34(6-7):421-9.

666 31. Yang C, Cao M, Liu Y, He Y, Du Y, Zhang G, et al. Inducible formation of leader
667 cells driven by CD44 switching gives rise to collective invasion and metastases in
668 luminal breast carcinomas. Oncogene. 2019;38(46):7113-32.
669 32. Cheung KJ, Padmanaban V, Silvestri V, Schipper K, Cohen JD, Fairchild AN, et
670 al. Polyclonal breast cancer metastases arise from collective dissemination of keratin
671 14-expressing tumor cell clusters. Proc Natl Acad Sci U S A. 2016;113(7):E854-63.
672 33. Karsch-Bluman A, Amoyav B, Friedman N, Shoval H, Schwob O, Ella E, et al.
673 High mobility group box 1 antagonist limits metastatic seeding in the lungs via reduction
674 of cell-cell adhesion. Oncotarget. 2017;8(20):32706-21.
675 34. Barbazan J, Alonso-Alconada L, Elkhatib N, Geraldo S, Gurchenkov V, Glentis A,
676 et al. Liver Metastasis Is Facilitated by the Adherence of Circulating Tumor Cells to
677 Vascular Fibronectin Deposits. Cancer Res. 2017;77(13):3431-41.
678 35. Eichbaum C, Meyer AS, Wang N, Bischofs E, Steinborn A, Bruckner T, et al.
679 Breast cancer cell-derived cytokines, macrophages and cell adhesion: implications for
680 metastasis. Anticancer Res. 2011;31(10):3219-27.
681 36. Cheung KJ, Ewald AJ. A collective route to metastasis: Seeding by tumor cell
682 clusters. Science. 2016;352(6282):167-9.
683 37. Padmanaban V, Krol I, Suhail Y, Szczerba BM, Aceto N, Bader JS, et al. E-
684 cadherin is required for metastasis in multiple models of breast cancer. Nature.
685 2019;573(7774):439-44.
686 38. Albergaria A, Ribeiro AS, Vieira AF, Sousa B, Nobre AR, Seruca R, et al. P-
687 cadherin role in normal breast development and cancer. Int J Dev Biol. 2011;55(7-
688 9):811-22.
689 39. Ribeiro AS, Sousa B, Carreto L, Mendes N, Nobre AR, Ricardo S, et al. P-
690 cadherin functional role is dependent on E-cadherin cellular context: a proof of concept
691 using the breast cancer model. The Journal of pathology. 2013;229(5):705-18.
692 40. Sridhar S, Rajesh C, Jishnu PV, Jayaram P, Kabekkodu SP. Increased
693 expression of P-cadherin is an indicator of poor prognosis in breast cancer: a
694 systematic review and meta-analysis. Breast Cancer Res Treat. 2020;179(2):301-13.

695 41. Vieira AF, Paredes J. P-cadherin and the journey to cancer metastasis. Mol
696 Cancer. 2015;14:178.
697 42. Dang TT, Esparza MA, Maine EA, Westcott JM, Pearson GW. DeltaNp63alpha
698 Promotes Breast Cancer Cell Motility through the Selective Activation of Components of
699 the Epithelial-to-Mesenchymal Transition Program. Cancer Res. 2015;75(18):3925-35.
700 43. Dongre A, Weinberg RA. New insights into the mechanisms of epithelial-
701 mesenchymal transition and implications for cancer. Nat Rev Mol Cell Biol.
702 2019;20(2):69-84.
703 44. Pearson GW. Control of Invasion by Epithelial-to-Mesenchymal Transition
704 Programs during Metastasis. J Clin Med. 2019;8(5).
705 45. Kroger C, Afeyan A, Mraz J, Eaton EN, Reinhardt F, Khodor YL, et al. Acquisition
706 of a hybrid E/M state is essential for tumorigenicity of basal breast cancer cells. Proc
707 Natl Acad Sci U S A. 2019;116(15):7353-62.
708

709

710 **Figure Legends**

711 **Figure 1. Defining gene signatures associated with IGF-1R expression and tumor**
712 **phenotype in human BCs. a.** Table of refined integrated WGCNA (IGF1R-GS2)
713 showing module and clinical trait association. Each row corresponds to a module
714 eigengene (ME), each column to a clinical measurement. Each cell contains the
715 corresponding correlation and p-value (in parentheses). The table is color-coded by
716 correlation according to the color legend. Green < 0 for negative correlation; Red > 0,
717 for positive correlation. **b-e.** Top 5 pathways identified by ingenuity pathway analysis
718 (IPA) revealing key signatures in 4 modules inversely correlated with IGF-1R
719 expression. (yellow module=cell cycle signature, greenyellow module=adhesion
720 signature, brown and tan modules=immune signaling signatures).

721

722 **Figure 2. Luminal loss of IGF-1R decreases tumor latency and increases**
723 **metastasis. a.** Schematic for luminal lineage IGF-1R knockout. **b.** Latency curve for
724 tumor development in Wnt1, DN-Wnt1, and K8iKOR-Wnt1 animals. For K8iKOR-Wnt1
725 animals, tumor latency is weeks post tamoxifen injection. *Statistic:* Mann-Whitney test **c.**
726 Growth curve after tumors arise until time of euthanization. *Statistic:* Non-linear
727 regression best fit for line slopes **d-e.** Graph of the percentage of animals **(d)** and table
728 of number of animals **(e)** with metastatic lesions after establishment of a primary tumor.
729 *Table Statistic*: Chi-square test; p=0.0251 for Wnt1 vs. DN-Wnt1 and K8iKOR-Wnt1. For
730 Wnt1 controls, vehicle and tamoxifen injected animals were combined as the
731 phenotypes were equivalent.

732

733 **Figure 3. Identifying mammary tumor heterogeneity by single cell RNA-**
734 **sequencing. a.** Uniform Manifold Approximation and Projection (UMAP) plot of cells
735 from Wnt1, DN-Wnt1, and K8iKOR-Wnt1 tumors resulting in 16 individual clusters. **b.**
736 UMAP plot with identification of cluster cell types defined by known markers. **c.** Dot plot
737 of cell markers. **d.** Percent tumor genotype graph for each cluster. Clusters are ordered
738 by identified tumor cells. MAC and T-cell populations were generally decreased in DN-
739 Wnt1 and K8iKOR-Wnt1 tumors. CAF populations were expanded in DN-Wnt1 and
740 K8iKOR-Wnt1 tumors. (MACS=monocytes/macrophages, TC=T cells, CAF=fibroblasts,
741 EPI=epithelial cells, EC=endothelial cells) **e.** IPA graphical summary of top pathway
742 alterations in DN-Wnt1 compared to Wnt1 tumors from Cluster 0 (MACs).
743 Blue=downregulated; orange=upregulated. **f.** IPA canonical pathways heat map of DN-
744 Wnt1 and K8iKOR-Wnt1 compared to Wnt1 tumors and the METABRIC brown (immune
745 signaling signature) module.

746

747 **Figure 4. Tail vein injections of primary tumor epithelial cells with reduced IGF-**
748 **1R. a.** Schematic of tumor epithelial cell tail vein injection. **b.** Top Row: Representative
749 whole lung images one-week after TVI of Wnt, DN-Wnt1, or K8iKOR-Wnt1 tumor
750 epithelial cells. Arrows denote macroscopic metastases. Bottom Row: Representative
751 lung hematoxylin and eosin staining for micrometastases from TVI of Wnt1, DN-Wnt1,
752 or K8iKOR-Wnt1 tumor epithelial cells. Scale bar = 50 microns. **c-d.** Micrometastases
753 **(c)** and macrometastases **(d)** counts from TVI lungs. *Statistic:* Non-parametric

754 Kolmogorov Smirnov test **e-f.** RNAscope immunofluorescence for the human IGF-1R
755 transgene (*dnIGF-1R*) in DN-Wnt1 TVI micrometastases 1 wpi **(e)** or in DN-Wnt1
756 endogenous primary tumor micrometastases (PTM) **(f)**. Scale bar = 50 microns **g.** RT-
757 PCR for the human IGF-1R transgene in sorted primary tumor cells from Wnt1 and DN-
758 Wnt1 tumors.
759
760 **Figure 5. Epithelial cell populations are altered with reduced IGF-1R. a.** UMAP plot
761 of re-clustering of epithelial cells from Wnt1, DN-Wnt1, and K8iKOR-Wnt1 tumors
762 resulting in 13 clusters. **b.** Heat map of top epithelial cell type markers. Top legend: top
763 row=tumor identity: gray=Wnt1, green=DN-Wnt1, pink=K8iKOR-Wnt1; Bottom
764 row=epithelial cell cluster. **c.** Dot plot of epithelial cell markers. **d.** Percent tumor
765 genotype graph for each cell cluster labelled with each cell type defined by markers.
766 (ALV=alveolar cell, LUM=luminal cell, DL=differentiated luminal cell, LP=luminal
767 progenitor, BAS=basal cell) **e.** Dot plot of alignment with metastatic signature. Arrows
768 depict clusters with high expression of markers indicating metastatic cell type. **f.** GSEA
769 plots for the epithelial mesenchymal transition (EMT) hallmark signature in Clusters E0,
770 E4, E6, and E10.
771
772 **Figure 6. Reduced IGF-1R reduces tumor cell growth and survival in lungs after**
773 **tail vein injection. a.** Schematic of tumor epithelial cell tail vein injection. **b.** Top Row:
774 Representative whole lung images after 3-, 6-, 8-, and 12-week TVI from Wnt1, DN-
775 Wnt1, or K8iKOR-Wnt1 tumor epithelial cells. Bottom Row: Representative lung

776 hematoxylin and eosin staining for micrometastases from TVI of Wnt1, DN-Wnt1, or
777 K8iKOR-Wnt1 tumor epithelial cells over time. **c.** Micrometastases (top graph) and
778 macrometastases (bottom graph) counts from TVI lungs over time. **d.**
779 Immunofluorescence for K8 (red), K14 (green), and phospho-histone H3 (pHH3, blue) in
780 metastases after 1wk TVI of Wnt1, DN-Wnt1, or K8iKOR-Wnt1 primary epithelial cells.
781 Scale bar = 50 micron; representative of n=3. **e.** GSEA plots of G2M and Mitotic Spindle
782 hallmark signatures in differentially expressed genes from DN-Wnt1 vs. Wnt1 epithelial
783 cell clusters. **f.** IPA canonical pathway heat map of differentially expressed genes from
784 DN-Wnt1 and K8iKOR-Wnt1 compared to Wnt1 tumors and the METABRIC (human)
785 yellow (cell cycle) module.
786
787 **Figure 7. Reduced IGF-1R function decreases tumor cell adhesion. a-c.**
788 Representative TVI lung staining for K8 (red) and K14 (green) from Wnt1 **(a)**, DN-Wnt1
789 **(b)** and K8iKOR-Wnt1 **(c)** 1 wpi mice. Dotted lines demarcate the metastatic lesions.
790 Arrows indicate double positive K8 and K14 cells. scale bar=50 micron; n=3. **d.** RT-PCR
791 for K14 in sorted luminal ($CD24^{+}/CD29^{lo}$) primary tumor cells from Wnt1, DN-Wnt1, and
792 K8iKOR-Wnt1 tumors showing increased expression in both IGF-1R models. *Statistic:*
793 Mann-Whitney U non-parametric t test. **e.** Measurement of adhesion from Wnt1 (grey),
794 DN-Wnt1 (green), or K8iKOR-Wnt1 (purple) by delta cell index over time for 6 hours
795 using the real-time xCELLigence assay. n=3; *Statistic:* Non-linear regression least
796 squares regression for slope best fit $p<0.0001$ for Wnt1 control compared to DN-Wnt1
797 or K8iKOR-Wnt1 **f-g.** Macrometastases **(f)** or micrometastases **(g)** counts in lungs from

798 TVI mice injected with Wnt1 or DN-Wnt1 tumor epithelial cells (250K), sorted luminal
799 epithelial cells, or sorted basal epithelial cells after 1 wpi. **h-i.** Representative H&E
800 images from Wnt1 **(h)** and DN-Wnt1 **(i)** lung micrometastases from TVI mice injected
801 with Wnt1 or DN-Wnt1 tumor epithelial cells cultured overnight at low adherence. **j-k.**
802 Micrometastases **(j)** and macrometastases **(k)** counts in lungs from TVI mice injected
803 with Wnt1 or DN-Wnt1 tumor epithelial cells cultured overnight at low adherence. **l-m.**
804 Immunofluorescence of K8 (red), K14 (green), and pHH3 (blue) in Wnt1 **(l)** and DN-
805 Wnt1 **(m)** TVI micrometastases from tumor epithelial cells cultured overnight at low
806 adherence. **n.** GSEA plots for the apical junction and apical surface hallmark signatures
807 from differentially expressed genes in DN-Wnt1 vs. Wnt1 epithelial tumor cell clusters.
808
809 **Figure 8. Altered cadherin expression in tumors with reduced IGF-1R. a.**
810 METABRIC data analysis for E-cadherin or P-cadherin in patient tumors with low IGF-
811 1R (IGF-1R z-score < -1) or high IGF-1R (IGF-1R z-score > 1) ($p < 2.0x10^{-16}$) *Statistic:*
812 Student's *t*-test. **b-c.** E-cadherin **(b)** and P-cadherin **(c)** expression in each epithelial cell
813 cluster identified with single-cell sequencing in Wnt1, DN-Wnt1, or K8iKOR-Wnt1
814 primary tumors. **d-m.** Representative images of E-cadherin (red) or P-cadherin (green)
815 immunostaining in Wnt1 **(d, g, j)**, DN-Wnt1 **(e, h, k)**, and K8iKOR-Wnt1 **(f, i, l)** primary
816 tumors. **m.** E-cadherin, P-cadherin, and double positive cell count graphs of primary
817 tumors. *Statistic:* One-Way ANOVA with Tukey's Multiple Comparison post-hoc test **n.**
818 Adhesion (delta cell index) over time in Wnt1 or DN-Wnt1 primary tumors with empty
819 vector (EV) or E-cadherin overexpression (Ecad). n=3; *Statistic:* Non-linear regression.

820 **o.** Adhesion (delta cell index) over time in Wnt1 or DN-Wnt1 with P-cadherin knockdown

821 (Pcad KD). n=3; *Statistic:* Non-linear regression.